![CHALMERS UNIVERSITY OF TECHNOLOGY]

Evaluation of a fluidized bed heat exchanger as a heat source in steam cracking process for olefins production

Modelling in Aspen Plus of steam cracking plant including reaction kinetics

Master's thesis in Sustainable Energy Systems

ANTHONY SALIBA

Department of Energy and Environment

Division of Energy Technology

Chalmers University of Technology

Gothenburg, Sweden 2017

Evaluation of a fluidized bed heat exchanger as a heat source in steam cracking process for olefins production

Modelling in Aspen Plus of steam cracking plant including reaction kinetics

ANTHONY SALIBA

CHALMERS

UNIVERSITY OF TECHNOLOGY

Evaluation of a fluidized bed heat exchanger as a heat source in steam cracking process for olefins production
Modelling in Aspen Plus of steam cracking plant including reaction kinetics
ANTHONY SALIBA

Supervisors: Viktor Stenberg, Department of Energy and Environment
Fredrik Normann, Department of Energy and Environment

Examiner: Magnus Rydén, Department of Energy and Environment

ABSTRACT

One of the main problems today is global warming and the need for more efficient energy use. Industry in general holds almost a third of global emissions and energy demand, and in turn the petrochemical industry holds a share of more than 30% of the industrial emissions. In specific, the production of olefins by steam cracking holds a significant share of the petrochemical CO_2 emissions and energy demand. Steam cracking involves highly endothermic reactions that require high temperatures and superheated steam to crack hydrocarbons (ex: ethane, naphtha…) into a combination of products including ethylene and propylene. The reactions occur in reactor tubes that hang inside a furnace and the required energy is provided by combustion of fossil fuels inside the furnace.

In this paper, a fluidized bed heat exchanger (FBHE) using metal oxides as active bed material (also referred to as oxygen carrier aided combustion or OCAC) was investigated as an alternative to the furnace used in today's steam cracking plants. The key advantage of a FBHE is its good heat transfer capability which allows for many potential benefits including lower temperature levels and less fuel consumption in the furnace. The advantages with active bed material include improved oxygen and fuel mixing in the dense bed (allowing more combustion to occur in the dense bed itself), use of very low excess air ratios, and achieving more uniform temperature distribution in the bed. A base case reflecting a typical ethane steam cracking process was chosen for reference and comparison with the FBHE alternative and the case was modelled in Aspen Plus. The focus of the model was the reactor tube, and a simplified reaction network and kinetics based on common and verified models from literature was used. However, the complete steam cracking plant layout and equipment were included in the Aspen model. Then an extensive literature review was conducted to select the FBHE dimensions, bed material, operating conditions, and heat transfer properties. The temperature required in the bed was then calculated and verified against the heat flux requirements in the reactor tube. The resulting temperature level, fuel consumption, and flue gas composition were noted to evaluate the benefits of using the FBHE. Finally, a sensitivity analysis on the heat transfer coefficient in the FBHE and on the reactor tube was conducted.

The study showed that with the fluidized bed heat exchanger with oxygen carrier aided combustion an excess air ratio of **1.03** and an outside heat transfer coefficient (h_{out}) of **600 W/m^2.K** could be used. As a result, the temperature in the furnace could be reduced by **194^{0}C** (down to 1064^{0}C) and fuel consumption by **48.5%** while maintaining the same operating conditions as the base case. Sensitivity analysis showed that increasing values of the outside heat transfer coefficient have a decreasing impact on the temperature and fuel consumption. For the reactor tube, sensitivity analysis showed that the coil outlet temperature (COT) has the biggest effect on ethylene yield. In addition, there is an optimum range of operation for the steam to hydrocarbon ratio and COT at which the ethylene yield is maximized.

Keywords: Fluidized bed heat exchanger, oxygen carrier aided combustion, olefins, steam cracking, heat transfer

Contents

Acknowledgements

I would first like to thank my supervisor Viktor Stenberg at the Department of Energy and Environment for constantly pushing me to do better through valuable feedback and comments.

I would also like to thank my examiner Magnus Rydén who always had his door open for my questions and concerns and for providing the necessary guidance to complete this work.

I would also like to acknowledge my colleagues at the thesis room for providing a nice and friendly working environment as well as the colleagues at the Department of Energy and Environment for always being ready to assist and contribute to this work in any way they can.

Finally, a big thank you to my family back home and my relatives in Sweden for their continuous support and encouragement.

Notations

Abbreviations

COT   Coil outlet temperature

FBHE   Fluidized bed heat exchanger

OCAC   Oxygen carrier aided combustion

S/HC   Steam to hydrocarbon ratio (kg/kg)

Symbols

A   Area (m^2)

d_i internal diameter of reactor tube (m)

d_t outer diameter of reactor tube (m)

d_p particle diameter (μm)

e_b emissivity of the bed

e_w emissivity of reactor tube wall

ε void fraction in the bed

g   acceleration due to gravity (9.81 m/s^2)

h_{out} Outside heat transfer coefficient ($W/m^2.K$)

h_{eq} equivalent heat transfer coefficient ($W/m^2.K$)

K_g Thermal conductivity of gas (W/m.K)

M_c molecular weight (kg/mol)

Pr   Prandtl number of the gas

ρ_c coke density or specific gravity (kg/m^3)

ρ_p particle density of bed material (kg/m^3)

Q   energy or heat flux (kW)

r_c rate of coking ($mol/m^2.s$)

t_c Coke thickness (m)

T_g Pyrolysis gas temperature (^0C)

T_f Furnace temperature

T_{fb}/T_b temperature of the bed (^0C)

T_{we}/T_w External reactor tube wall temperature (^0C)

U	superficial gas velocity through bed (m/s)
U_{mf}	minimum fluidization gas velocity (m/s)
μ	dynamic viscosity of gas (N.sec/m^2)

1. INTRODUCTION

Global warming and fossil fuel consumption are part of the key issues facing societies across the world. High levels of CO_2 emissions are increasing CO_2 concentrations in the atmosphere which is the main contributor to global warming. Sources of CO_2 emissions are varied and include power production, transport, and industry. Across these sources, the common denominator is high energy demand and using that energy more efficiently can save a lot of emissions. Industry in general holds close to a third of global energy demand and CO_2 emissions [1]. A large share of more than 30% of industrial energy demand comes from the chemical and petrochemical sector in specific, and hence the need to improve energy efficiency and emissions in this sector [1].

The petrochemical industry refers to chemical products derived mainly from petroleum (but also other fossil fuels), and is split into two main classes: olefins and aromatics. Light olefins are high value chemicals that serve as the main raw material for the petrochemical industry and production of various materials. The materials include several plastic products, synthesis fibers, polymers, and rubbers. Light olefins refer to the class of unsaturated hydrocarbons with a single double bond and a chemical formula C_nH_{2n} [2]. The main components of light olefins are ethylene and propylene, with chemical formulas C_2H_4 and C_3H_6 respectively. Also these two compounds represent the largest volume of produced olefins, and as such are the most interesting to study [3] [4]. Today the ethylene and propylene production industry is very large with a yearly demand of around 155 million tons of ethylene [5] and 100 million tons of propylene per year [6]. This demand has been increasing over the last couple of years and is expected to continue to grow [4] [5] [6]. Accordingly, the need for more efficient production processes with a lower carbon footprint is still a priority.

For the production process of olefins, the two most common paths are fluid catalytic cracking (FCC) and steam cracking. FCC takes up nearly 60% of the global feedstock volume and is used in oil refineries, while the remaining 40% are used in steam cracking in dedicated plants [6]. The volume of hydrocarbon feeds for production of olefins in 2014 was around 1,000 million tons, with around 390 million tons going to steam cracking plants [6]. FCC requires relatively low temperatures and heat input, and the main reactions proceed with the help of a catalyst to reach the end product. As such, the catalyst is the main focus in a FCC process. Steam cracking on the other hand is much more energy intensive and requires significant amounts of heat for the desired endothermic reactions to proceed. The focus in steam cracking is then the heat source, which is typically a flame burner furnace. Steam cracking occurs at high temperatures in the range of 700-1000^{0}C [5]. Heat is generated through combustion of fossil fuels. Ethylene is almost exclusively produced in steam cracking plants, while 50% of propylene is produced in such plants [6]. In FCC plants, gasoline is the main product with olefinic gases (converted to propylene), oil distillates, and butane and propane as by-products. The feedstock for production of ethylene are hydrocarbons, namely naphtha, ethane, gas oil, and liquefied petroleum gas (LPG) [6]. The largest feedstock volumes come from naphtha and ethane (around 82% in 2002 [7]) and this paper will focus on ethane due to relatively simpler reaction kinetics. For propylene, the main feedstocks are naphtha and gas oil [6]. Figure 1 below illustrates the relation between FCC, steam cracking, ethylene, and propylene.
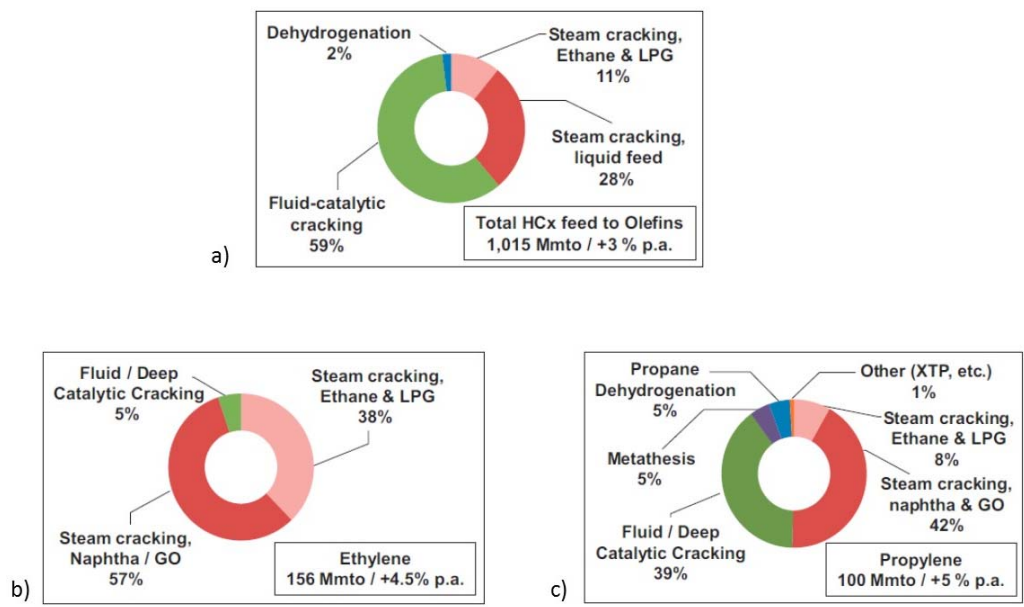
a)

b)

c)

Figure 1. a) hydrocarbon feed used for olefin production processes. b) Ethylene production by source. c) Propylene production by source [6]

In a steam cracking plant, the process from feedstock to olefins involves many steps. A typical process block diagram is shown in Figure 2.
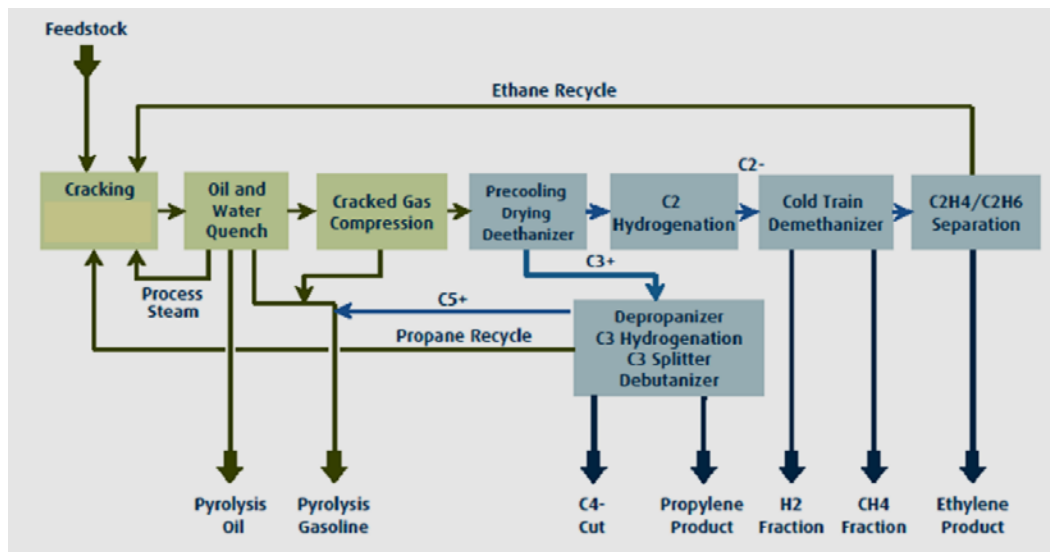
Figure 2. Block diagram for typical steam cracking process [8]

The process used in this paper will be discussed in more detail in section "4. Process". The first step in the steam cracking process and one of the key components is the furnace, and it is where the primary reactions occur. The furnace configurations typically found today have flame burners distributed along the furnace walls that are fed with fuel and excess air to provide the required heat transfer to the reactor tube hanging inside the furnace. Such a furnace is depicted in Figure 3. The

radiant section is where heat is supplied to the reactor tube and a convection section where energy recovery from the hot flue gases occur.

Figure 3. Illustration of a furnace including the different sections [5]

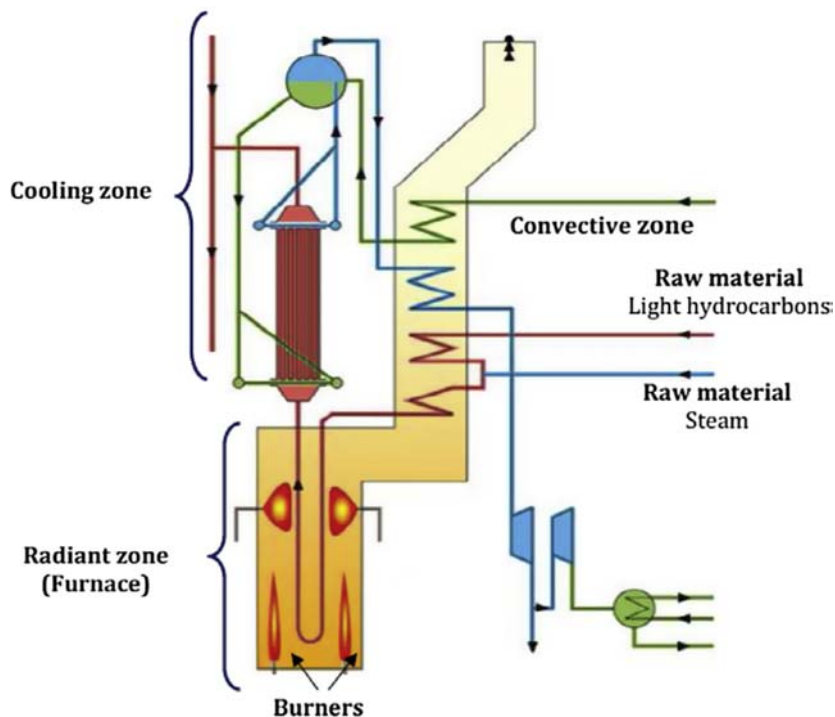Heat transfer conditions in the radiant zone of typical industrial furnaces with flame burners require the temperature in the furnace to be as high as 1300^0C to achieve the desired temperatures in the reactor tube. Due to the high temperatures required, issues like heat loss from the furnace, high consumption of fuel, CO emissions, and material heat stress are present. This report investigates the potential of addressing these drawbacks by using a fluidized bed heat exchanger with oxygen carrier aided combustion (FBHE-OCAC) as an alternative heat source. The fluidized bed potentially offers better heat transfer conditions which should reduce the temperature levels required in the furnace and the drawbacks that come with it. Also the temperature gradients are lower in a FBHE due to very efficient heat transfer within the bed. The active bed material, also referred to as oxygen carrier aided combustion or OCAC, offers several benefits of which the most important is enabling high levels of fuel conversion in the dense bed itself rather than the freeboard above the bed. This in turn allows the bed to reach the required temperatures and provide the necessary heat for the endothermic reactions in the reactor tubes. In addition, OCAC has the potential to decrease excess air requirements compared to inert beds and furnaces with flame burners which in turn decreases auxiliary power requirements for fans/compressors. Ultimately, combining the FBHE with the OCAC concept should improve energy and fuel efficiency of the steam cracking process, reduce CO emissions, and provide unchanged levels of ethylene and propylene yields. To assess the potential of the FBHE a base case for ethane cracking was selected as a reference and for comparison. Then the FBHE design and operating conditions were decided upon using a comprehensive literature review. In addition, the entire steam cracking process was modelled in Aspen Plus which allowed the simulation of different operating conditions.

2. AIM

Given the large energy demand of the petrochemical industry, the broader aim is to investigate the possibility of a more sustainable steam cracking process for olefin production. Up to the author's knowledge, the FBHE-OCAC as a heat source for olefin production by steam cracking is a novel idea that has not been covered in literature. As such, the specific aim and main effort was to suggest a design for a FBHE that can replace industrial furnaces used in steam cracking plants and evaluate the feasibility and potential benefits of using the FBHE. The design of the FBHE was based on extensive literature review and included geometry, heat transfer conditions, excess air ratio, and bed material while the temperature, CO emissions, and fuel flow rate in the bed were determined mathematically. In addition, a model for the complete steam cracking process was developed in Aspen Plus with a focus on reaction kinetics in the reactor tube. The purpose of the model was to complement the study by providing a complete picture of the steam cracking process and to serve as a tool for predicting the output of olefins and evaluating the effect of changes in operating conditions of the reactor coil. Finally, a sensitivity analysis was performed on both the outside heat transfer coefficient in the FBHE and the reactor tube in the Aspen model.

This thesis will hopefully be of significant value for industries looking to use alternative and more efficient heat generation sources in their steam cracking plants as well as a base case for further, more detailed development of the Aspen model. The results of the design and simulations will provide a background for further research on the FBHE application in steam cracking. In addition, the model has the potential to be upgraded and applied for reactor and furnace control, optimal feedstock selection, and production planning.

3. SCOPE

In this paper the focus was on the FBHE. First a base case for steam cracking of ethane was selected to be used for the design of the FBHE and development of the model in Aspen Plus. Ethane was chosen instead of naphtha as a feedstock since determining the exact composition of naphtha fuels is challenging and the kinetic model for steam cracking of naphtha is complicated and includes many free radical reactions which are hard to integrate in Aspen Plus. Next the design of the FBHE was determined. As mentioned above, the design included geometry (dimensions), heat transfer conditions, excess air ratio, and bed material. For the heat transfer, previous research on FBHE with similar conditions as those in this paper was used to identify a suitable heat transfer coefficient. No model or calculations for the heat transfer were made due to the complexity of the topic, and it was assumed that there is one constant heat transfer coefficient in the bed. The fluidization velocity was assumed to be at optimal based on literature reviews without doing explicit calculations. Power requirements for the fans/compressors that supply the air were not taken into account in the energy savings calculations. The temperature in the bed was assumed to be uniform and was calculated accordingly. The composition of the combustion flue gases and CO emissions in the FBHE were calculated using the model in Aspen Plus and compared with measured CO emissions in experimental studies.

As for the reactor coil, it was modeled as a plug flow reactor in Aspen Plus. The kinetic model of the reactions were based on a simplified 8-reaction model from literature and followed the Arrhenius Powerlaw type of reactions. A coking model was not included and evaluated in this study. Instead the effects of coking on energy and temperature in the furnace and FBHE were considered, and those effects were taken from the results in the base case which does include a coking model. The temperature profile inside and on the skin of the reactor tube was kept the same as the base case

rather than calculating the same, and the energy requirements were based on the simulation done in the base case.

4. OLEFIN PRODUCTION PROCESS

The first step in the process is the furnace where steam and hydrocarbon feed are mixed and pre-heated in the convection section before entering the radiant section of the furnace. Typical pre-heat temperatures are up to 650^0C [9]. Steam is used to dilute the feed, reduce the partial pressure of the feed, and help in reducing coke formation on the inside of the reactor tube walls. Steam to hydrocarbon ratio depends on the feed. An example range for ethane is 0.3-0.4 kg steam/kg hydrocarbon and for naphtha 0.6-0.7 kg/kg hydrocarbon [9]. The mix enters the furnace in a reactor tube. Inside the reactor tube the cracking reactions occur, and several important parameters are considered. The hydrocarbon undergoes a large variety of reactions (up to 500 reactions producing 90 radicals) [10]. The reactor skin or wall temperature is in the range of 850-1100^{0}C [5]. Special material like Inconel 600 is used to withstand the thermal stress and usually plants have an upper limit on the tube wall temperature to prevent breakdown of the reactor coil. The temperature of the feed gas inside the reactor tube increases along the length of the reactor with the range from beginning to end being from 650-900^{0}C. The temperature of the feed gas is controlled to maintain selectivity towards olefins production, and the control is done by measuring the temperature at the outlet of the reactor tube, also called coil outlet temperature in literature or COT [9]. Another parameter is the residence time in the reactor. The residence time is controlled to make sure reactions proceed far enough to produce as much desired product as possible, since after a certain time the cracking reactions will continue which significantly changes the composition of the cracked gas. For older existing plants the residence time is in the range of 0.2-0.8 seconds, but more modern plants have even shorter residence times in the range of 0.08-0.25 seconds [5]. Residence time is dependent on the temperature at which the reactions occur. Higher temperatures, which give higher yields, mean faster reaction velocities, and accordingly the residence time becomes lower. Also at the same temperature level, shorter residence times mean lower coke deposition rates [10]. The feed flow rate and tube diameter are used to control the residence time. An example feed flow is 11600 kg/h [9]. Finally, total pressure of the feed mix affects selectivity of the reactions (and with it the yield) and usually low pressures are favored in the range of 170-250 kPa [5]. Pressure drops in the reactor (difference between inlet and outlet) are in the range of 70-150 kPa [5]. An example industrial plant used is Arak Olefin plant, part of Arak petrochemical complex in Iran [9]. The Arak plant is a modern steam cracking plant and has the typical configuration for such plants as found in literature and other industrial examples. In the Arak plant, for a reactor tube length of 45m, the pressure drop was 65 kPa [9]. Reactor tube length can be in the range of 10-100 m with a 3-15 cm range in diameter [5]. Figure 4 illustrates the distribution of temperatures in the furnace of a typical steam cracking plant.
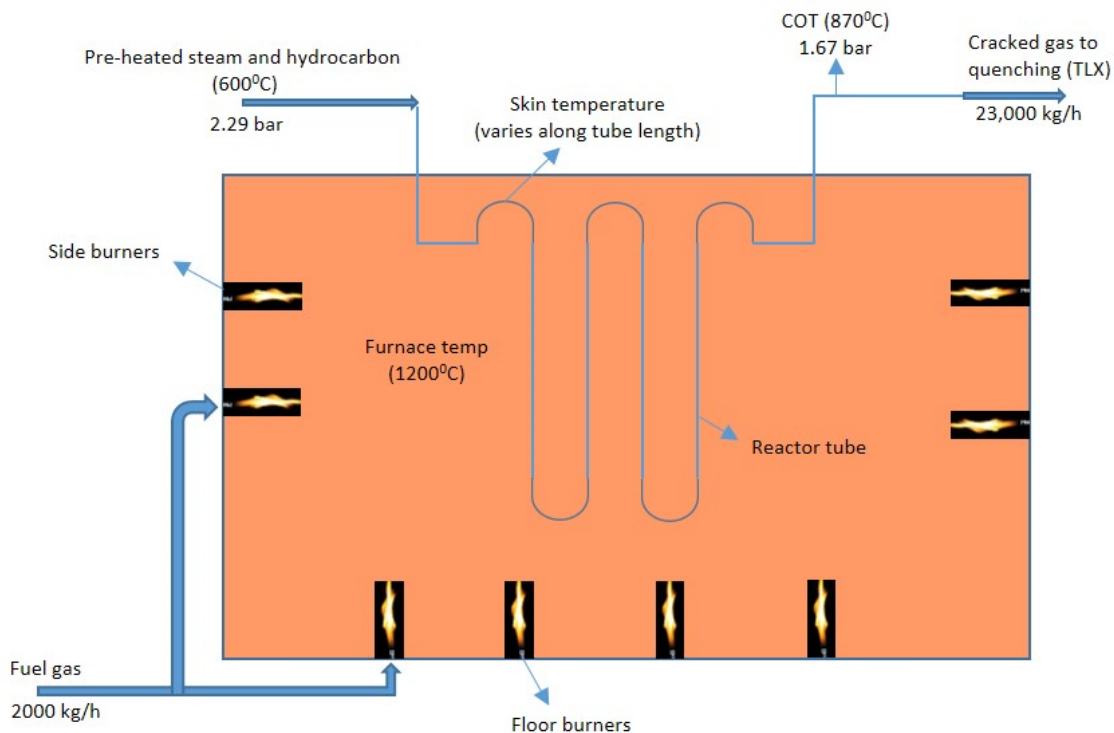
Figure 4. Example furnace radiation section with temperature data

Inside the radiant section of the furnace, fuel combustion maintains the temperature at the required level for the chemical reaction in the reactor tube to proceed. Typically, the temperature range is 1000-1300°C [5]. The most common fuel compositions have CH_4 (natural gas) as the main component, in addition to H_2, CO, and traces of light olefins which are recycled from downstream of the process [5]. Excess air is added to the fuel feed and fed to the burners. An example fuel composition from Arak plant by weight percent is 86% CH_4, 14% H_2, and 15% excess air [9]. The furnace dimensions in the Arak plant are 11.47 m height, 10.48 m length, and 2.1 m depth [9]. An important factor in the furnace is the heat transfer conditions or the heat flux to the reactor tube. In the radiant section, the bulk of the heat is transferred by radiation, and hence the name. The flame burners are distributed along the furnace walls to achieve the temperature gradients and heat flux required.

After the furnace comes the transfer line exchanger (TLE, also referred to as TLX), where rapid quenching of the cracked gas occurs to freeze further undesired reactions from occurring. These reactions lead to formation of heavy polymerization products and an increase in the gasoline content of the cracked gas which mean a reduction in the light olefin (ethylene and propylene) content. Next comes the caustic tower where H_2S gases are scrubbed from the cracked gas. In the case of pure ethane feedstock this step can be skipped since there are no sources of sulfur present. Then the dryer is used to remove water/steam content from the gas by condensation. Afterwards, the splitting columns are used to separate the cracked gas (also called pyrolysis gas) into the different required products. The De-C3 column separates C4 cuts from the pyrolysis gas which are a mixture of C4 hydrocarbons consisting mainly of 1,3-Butadiene (C_4H_6) [11]. Butadiene is used primarily as a chemical intermediate and as a monomer in the manufacture of polymers such as synthetic rubbers or elastomers [11]. In turn, these rubbers and their latexes are used to produce other goods and

materials such as tires, gloves, and gaskets [11]. The De-C1 column separates methane and hydrogen which can be recycled to the furnace as fuel. The De-C2 column separates C3 cuts which consist mainly of propane (C_3H_8) and propylene (C_3H_6). Propane is used in applications such as fuel for engines, gas torches, and gas stoves. The remaining stream consists of Acetylene (C_2H_2) and Ethylene (C_2H_4). Acetylene combustion with oxygen produces high flame temperatures (over 3,300^{0}C) which is used in applications such as welding and cutting of steels, and acetylene is also used to produce acrylic acid derivatives that are in turn used to form acrylic fibers, glasses, and paints. Figure 5 illustrates those steps for an ethane cracking plant [12].
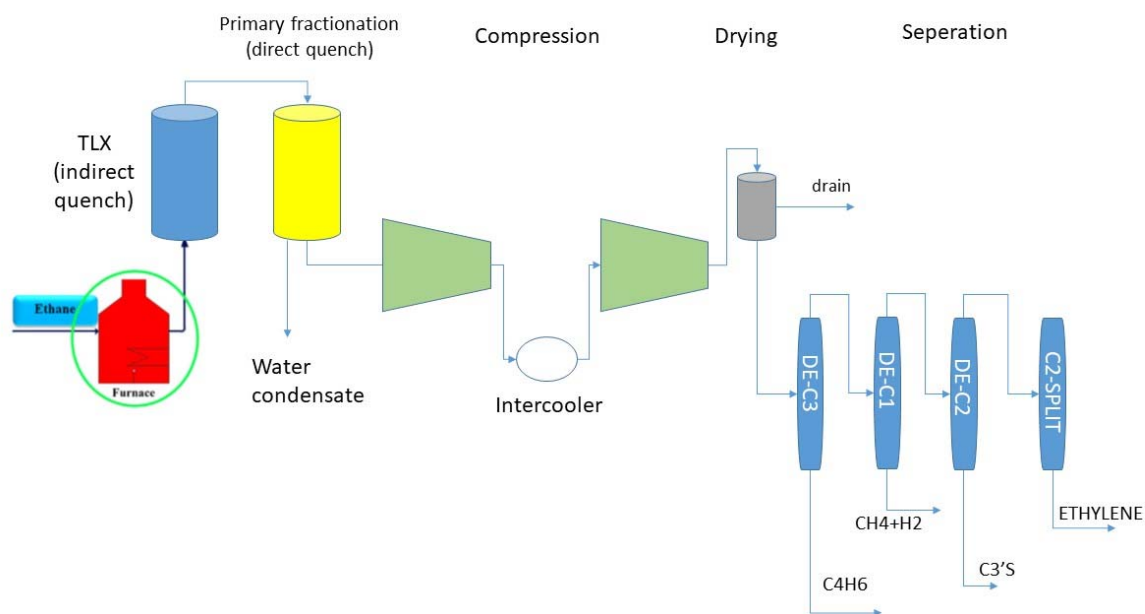

Figure 5. Equipment flowsheet for a typical ethane steam cracking plant [12] [13]

4.1 Base case for steam cracking of ethane

Steam cracking of ethane has been investigated for some time in literature. Recent studies focus more on the kinetic model for the pyrolysis reactions and on optimizing yields and operating conditions. As such, details about the heat transfer and temperature profiles in the furnace are often not presented in those studies. After a comprehensive literature review, the data provided in the paper by Plehiers et al. [13] was selected to establish the base case for this study. The paper includes almost all information required to build a model, especially the temperatures and temperature profiles in the furnace and reactor tube. In addition, the paper simulates a typical industrial furnace with typical operating conditions that are closely matched in several other studies on the subject [12] [14] [15]. Also the paper compares the results to an actual plant and confirms agreement within acceptable tolerances. Finally, the paper takes into account coking which is interesting to consider for this research as coke acts as a barrier to heat transfer. This causes the temperature in the furnace, and with it the energy requirements, to increase. The first set of information extracted from the paper is the furnace characteristics. The dimensions of the furnace were used as a comparison to the determined FBHE dimensions. However, those dimensions were not relevant for the model in Aspen Plus. Table 1 shows the furnace characteristics for the base case:

Table 1. Furnace characteristics for base case

Length	9.6 m
Depth	1.8 m
Height	12.73 m
Fuel composition	
Methane	95 vol %
Hydrogen	5 vol %
Excess air	20%

The maximum temperature in the radiation section is not specified in the base case paper. Instead the average temperature (along the length of the furnace) of the flue gas at the exit of the radiation section is shown, and it is 1116^0C which is 266^0C higher than the COT temperature. The issue with the temperature at the exit of the radiation section is that it reflects the temperature after all the heat transfer to the tube has occurred, and as such is lower than the temperatures present along the furnace height. To find a better approximation of the expected temperature differences present between the furnace and external tube wall, several studies on naphtha cracking furnaces were reviewed where the temperature profile along the height of the furnace is simulated. The studies used in this paper are by G. Hu et. al. [16] [17]. The use of those two studies is justified by very similar furnace and reactor coil configuration, and coil inlet and outlet temperatures and pressures. Based on those studies, the temperature difference at maximum heat flux between furnace gas and external tube wall was assumed to be 300^0C.

The second set of information was the reactor tube geometry, operating conditions, and the temperature profile of the pyrolysis gas. This information is shown in Table 2 and Figure 6, and is one of the main inputs for the Aspen Plus model.

Table 2. Reactor tube details

|	
Coil total length	100 m
Coil inlet temperature	656^0C
Coil outlet temperature (COT)	850^0C
Coil Inlet pressure	292 kPa
Coil outlet pressure	195 kPa
No. of passes	8
Internal diameter passes 1-6	12.4 cm
External diameter passes 1-6	14 cm
Internal diameter passes 7-8	13.6 cm
External diameter passes 7-8	15.2 cm
Tube thermal conductivity	$-1.257 + 0.04327T$ (W/m.K)
Feedstock	100% ethane
Hydrocarbon feed rate	2800 kg/h
Steam dilution	0.365 kg steam/kg hydrocarbon
Coke conductivity	6.46 W/m.K
Coke specific gravity	1600 kg/m3
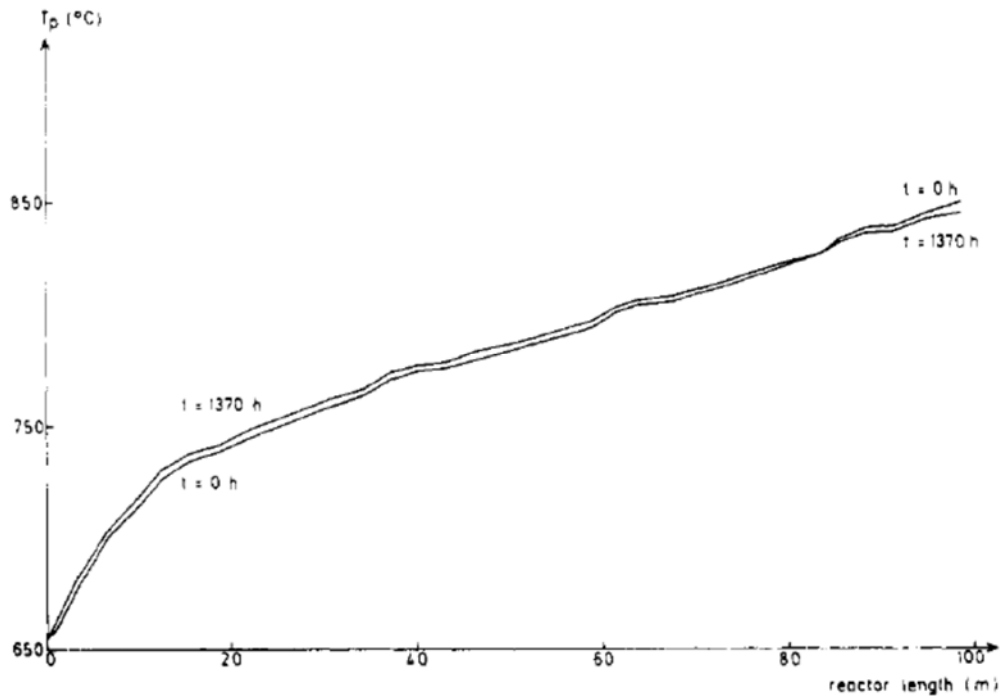
Figure 6. Temperature profile along the reactor tube (T_g) [13]

For Figure 6, it can be seen that there are two temperature profiles for 0 hours of operation and 1370 hours of operation. The difference between the run times is the thickness of the coke layer formed on the inside of the reactor tubes which increases with time, and in turn slows the heat transfer to the pyrolysis gas. So as more coke is formed the temperature of the pyrolysis gas decreases for the same heat flux. For the temperature profiles, they are almost the same for the entire run length since the assumption in the paper is that the heat supplied to the tube is adjusted to keep the temperature levels of the gas the same.

The third set of information was the heat flux profiles and external tube temperatures along the reactor length for different run length of the reactor. These profiles are shown in Figure 7 and Figure 8. The 0 h and 1370 h graphs were compared to evaluate the effect of coke formation, and the 1370 h case was used to verify that the coke model detailed in the section below was working well. Looking at the graphs in Figure 7, it can be seen that the heat flux to the tube varies a lot with several spikes and dips. This profile is due to many reasons. One of the reasons is the proximity of the flame and the distribution of flame burners along the wall of the furnace which cause an increase in the heat flux. The other is the combination of temperature difference between furnace and tube and the rate of the reactions inside the tube. The temperature difference can be seen as the driving force which decreases as the temperature of the tube increases. The reactions start slow at the beginning of the tube and become more intense towards the middle, then slow down a bit towards the end. More intense reactions consume more energy and thus require higher heat fluxes.
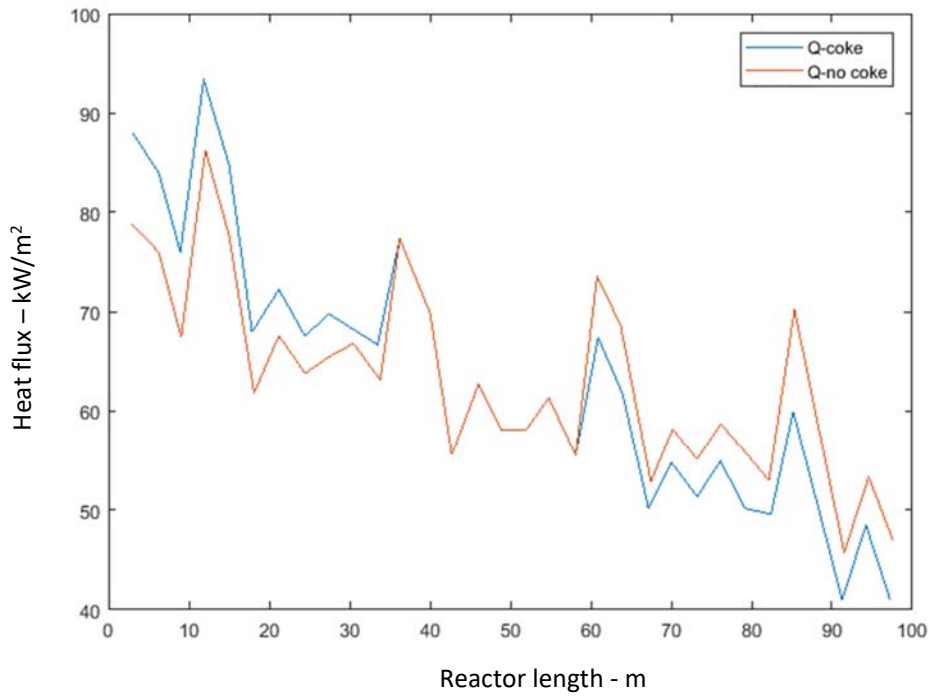
Figure 7. External heat flux on reactor tube [13]

Looking at Figure 7, the heat flux for the coke case is higher than the baseline at the beginning of the reactor tube since little coke is present while it is lower at the end of the reactor tube where coke is present. Overall, the average heat flux is almost the same for both cases. This matches with the fact that the temperature profile inside the reactor tube is also the same for both cases, which means the same intensity of cracking reactions is taking place.
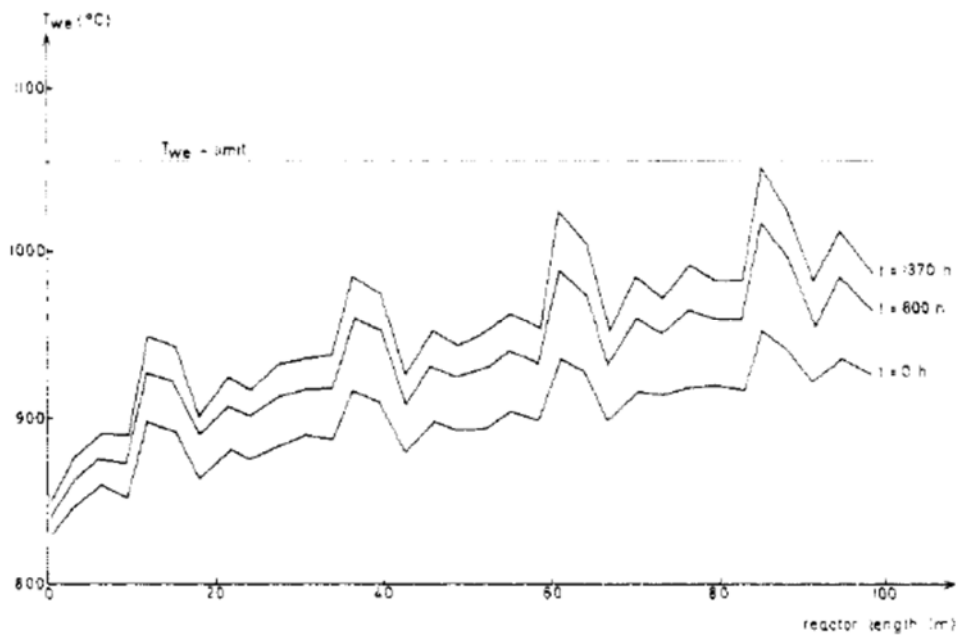

Figure 8. Reactor tube skin (external wall) temperature profile T_{we} [13]

19

The issue with the base case paper was the kinetic model used to simulate the cracking reactions, which is detailed and includes up to 150 reactions. In Aspen Plus, it is difficult to incorporate such a large number of reactions and include radicals and generic molecule formations (such as C_nH_{2n-1}). Instead, a simplified reaction network of 8 reactions from Shokrollahi et. al. [12], which is based on Sundaram and Froment [18], was used. The reactions and related Arrhenius parameters are listed in Table 3 and Table 4 respectively. The rate of the reaction is then $k = Ae^{-\frac{E}{RT}}$. Reactions 1 and 5 below are reversible, and the rates for the reverse reactions were calculated from Shokrollahi et. al. [12] and checked against the rates given in P. Ranjan et. al. [15]. The Arrhenius parameters for the reverse reactions are shown in Table 5. Tables 3, 4, and 5 represent the simplified kinetic model used in this paper. This kinetic model as well as models from P. Ranjan et. al. [15] and M.N. Rosli et. al. [19] were implemented in Aspen Plus. The results showed that the three models gave very similar predictions of the final product composition. In addition, the percentage difference between the predicted yields using the simplified kinetic model and the yields from the base paper was calculated. The maximum difference was found in the conversion of ethane, which amounted to 9%. This error percentage is acceptable for the purpose of this thesis, especially that coking reactions were not accounted for. Thus it was considered satisfactory to adopt the simplified kinetic model.

Table 3. Simplified reaction network for cracking of ethane

$C_2H_6 \leftrightarrow C_2H_4 + H_2$	(1)
$2C_2H_6 \rightarrow C_3H_8 + CH_4$	(2)
$C_3H_8 \rightarrow C_3H_6 + H_2$	(3)
$C_3H_8 \rightarrow C_2H_4 + CH_4$	(4)
$C_3H_6 \leftrightarrow C_2H_2 + CH_4$	(5)
$C_2H_2 + C_2H_4 \rightarrow C_4H_6$	(6)
$2C_2H_6 \rightarrow C_2H_4 + 2CH_4$	(7)
$C_2H_6 + C_2H_4 \rightarrow C_3H_6 + CH_4$	(8)

Table 4. Arrhenius parameters for simplified reaction network

Rate Coefficient	A (s^{-1}) or (m3.mol^{-1}.s^{-1})*	E (kJ/mol)
k_1	$4.65 \cdot 10^{13}$	273
k_2	$3.85 \cdot 10^{11}$	273
k_3	$5.89 \cdot 10^{10}$	215
k_4	$4.69 \cdot 10^{10}$	212
k_5	$6.81 \cdot 10^{8}$	154
k_6	$1.03 \cdot 10^{12}$*	173
k_7	$6.37 \cdot 10^{23}$	530
k_8	$7.08 \cdot 10^{13}$*	253

Table 5. Reverse reaction rates

Reaction	A (s^{-1})	E (kJ/mol)
$C_2H_4 + H_2 \rightarrow C_2H_6$	$8.49 \cdot 10^8$	136.5
$C_2H_2 + CH_4 \rightarrow C_3H_6$	$3.81 \cdot 10^8$	147.2

With the above information, the most important parts of the ethane cracking plant, the furnace and reactor coil, were ready to be modeled. The rest of the process downstream is often not considered or focused on in literature due to two factors: the equipment is almost the same with regards to design and operating conditions (with some exceptions for the TLE); the equipment serve the purpose of separating the streams into required products very well and not much room for improvement is available. As such, it is assumed in this paper that the downstream components shown in Figure 5 apply. The pressure and temperature details for each component were based on several literature sources [13] [12]. This leaves the coking model and some key assumptions made to be able to proceed with the implementation in Aspen Plus, which are detailed in the following sections.

4.1.2 Coke formation

In steam cracking for olefins production, coke is solid carbon deposits on the internal reactor tube walls. Coke layers affect the temperature of the tube skin, internal tube diameter, and product yields. Coke layers act as a thermal barrier to heat transfer from the furnace to the pyrolysis gas. Since temperature profiles of the pyrolysis gas is of major importance for product yield and selectivity, plant operators would like to keep the profile constant as much as possible. Accordingly, as the coke layer becomes thicker the amount of heat required to obtain the same pyrolysis gas temperature will increase. This in turn raises the temperature on the tube skin, which causes thermal stress on the tube material. The metal has a temperature limit, usually around 1100^{0}C [13] [12], and that means the furnace has to be taken offline to de-coke the reactor tube before it can be operated again. The most common options for de-coking are using a mixture of air and steam to burn off the coke and using a pig that travels through the pipe and removes the coke layer. For the tube diameter, the coke layer reduces the internal diameter which in turn reaches a limit and causes operations to be stopped for de-coking. Due to these two factors, the run length of the plant falls in the range of 30-80 days, and in the base case paper it is 57 days (or 1370 h).

With regards to product yields, coke formation reactions affect the composition of the pyrolysis gas at the outlet of the reactor tube. The rate of formation of coke depends on the temperature and the concentration of coke precursors in the pyrolysis gas, as well as operation time. Higher temperatures and concentrations of coke precursors lead to higher rates of coke formation. Most important coke precursors in steam cracking of ethane are ethylene, propylene, and 1,3-butadiene [12]. Those precursors are also in agreement with papers on steam cracking of naphtha which identify the same groups of molecules as precursors [20]. Since temperature and coke precursor concentration are much higher further along the reactor length than at its start, coke thickness is highest in the final sections of the reactor. This should be one of the reasons why the tube internal diameter becomes larger in passes 7 and 8 as shown in Table 2. After 57 days of operation, the coke thickness in the base case becomes 13.4 mm at 80 m of the reactor length (which corresponds to passes 7 and 8). As discussed above, the internal diameter affects the run length of the plant, and so increasing the diameter by 12 mm in the last passes compensates for the coke layer build up. As for operation time, the thickness of the coke layer increases with time as coke reactions continue to build up that layer.

Due to the complexity of coke formation, time dependence of coke deposits, and the nature of the coking reactions it was difficult to get an accurate prediction of the concentration of coke using the Aspen Plus model. For the purposes of this thesis, coking reactions were not taken into account. The composition of the pyrolysis gas after the reactor tube was found to be well within range of the base case paper and the industrial values, and accordingly the coking reactions were not required for this paper. Instead, the focus was kept on the effect of the coke layer on temperature and energy demand.

4.1.2 Assumptions
The main assumptions made in this study are listed below. The assumptions are based on the base case paper as well as previous work where the same assumptions are widely accepted [17] [13] [5].

- Reactor modeled as 1-dimensional plug flow reactor
- Gas flow mixture behaves as an ideal gas
- Radial concentration gradients are neglected

5. METHOD
This section shows the detailed procedure followed to obtain a functional model of an ethane steam cracking plant in Aspen Plus. The approach was first to implement the base case data into an Aspen Plus model that can accommodate input changes easily. With the model ready, simulation proceeded and key parameters were noted to be used as performance indicators. The key parameters, collectively referred to as "results" hereon after, were:

- Energy demand in the reactor tube (unit: W)
- Fuel consumption (kg/s)
- Ethylene yield (kg C_2H_4 /kg C_2H_6)
- Methane yield (kg CH_4/kg C_2H_6)
- CO_2 and CO emissions (ton/yr and ppm respectively)

The energy demand in the reactor tube was calculated by Aspen as the sum of the difference in enthalpies of formation of the different compounds in the gas. Fuel consumption was determined as the mass flow rate of fuel (methane) required to meet the energy consumption at a certain temperature. The combustion reaction of methane was considered in Aspen using the RGibbs block which calculates the equilibrium composition of the flue gases and energy released per kg of fuel at a specified temperature. Since temperature level and energy released are considered in the RGibbs block, it was also used to represent the FBHE. The temperature, fuel flow, and air flow were set as an input to the block, and the released energy and flue gas composition were noted. For the base case the fuel consumption is determined based on the fired duty specified in the base case paper, which takes into account losses in the furnace. For the FBHE, the energy required is considered to be the same as the energy demand of the reactor tube. For the emissions, as mentioned the block calculates the equilibrium composition of the flue gas. In practice, flue gas from furnaces and boilers do not reach full equilibrium, which means higher CO concentrations will in reality be present in the flue gas as compared to the output from the RGibbs block. Accordingly, the CO_2 and CO concentrations from Aspen Plus were used for comparison between the different cases rather than true values of expected emissions from the combustion conditions. Finally, the ethylene yield is determined from the output of the Rplug block in Aspen which is used to simulate the reactor tube.

Afterwards, the sensitivity analysis was conducted on the model to identify which parameters have the biggest impact on the energy efficiency of the process. This was done by varying one parameter

over a range of values while keeping other parameters the same, and taking note of the results for each value of the parameter. The key parameters studied, collectively referred to as "variables" here on after, were:

- Outside heat transfer coefficient in FBHE (h_{out}): varied between 300-900 W/m^2.K
- Steam to hydrocarbon ratio (S/HC): Varied from 0.2-0.8 kg/kg
- Coil outlet temperature (COT): Varied from 800-950^{0}C. Since the reactor has a temperature profile rather than a single temperature, it was assumed that each point of the profile shifts vertically by the same amount that the COT has shifted.
- Pressure of the feed: The pressure drop over the reactor was assumed constant, and the inlet pressure was varied from 320-220 kPa.

The parameters noted for comparison were the "results" defined above. Afterwards, the design of the FBHE was performed under the guideline that it should be a suitable replacement for the conventional furnace. The parameters determined for the FBHE are comprehensive, and include geometry, bed material composition, excess air ratio, and heat transfer coefficient. Then the temperature level required in the FBHE was calculated and verified against the temperature profile of the pyrolysis gas.

5.1 Aspen Plus model

Aspen Plus is a flow-sheeting software that simulates chemical processes. The advantage of Aspen is that is a visual tool, relatively simple to use since complex calculations are built in and the user only specifies the input data, and allows for integration of whole processes. Aspen represents different components of a plant or process as blocks that interact with each other using streams. Each type of block represents a specific method used to handle the input data, and the user chooses the block based on the output requirements. Streams represent material flows in and out of the block, and are used to show the temperature, pressure, and species compositions.

The first element to be modeled was the reactor tube. The reactor tube was modeled as a one dimensional plug flow reactor with an imposed temperature profile. The block used was Rplug. The input stream to the block was the ethane and steam mixture at the specified flowrates, temperature and pressure. Next the pressure drop was specified, and then Aspen assumes a linear pressure profile along the reactor tube length using the input and output pressure. In Aspen the property method should be specified and that is an input that tells Aspen which set or table of thermodynamic and chemical data to use for the calculations. For selecting the property method, M.N. Rosli et al. [19] tried several property methods and showed that the results are very similar, eventually adopting the GRAYSON property method since it is also recommended by Aspen for ethylene production applications. As such the GRAYSON property method was also used in this paper. Then the reactions and kinetic parameters shown in Tables 3 and 4 were entered. The reaction type was defined as a Powerlaw reaction.

The second element was the combustion in the furnace. The block RGibbs was used to simulate the combustion of CH_4. The RGibbs block uses the Gibbs free energy minimization to calculate equilibrium compositions of a reaction at a certain temperature. The inputs to the block are the flow rates, temperature, and pressure of the fuel and air mixture. The outputs are the composition of the flue gas and the net energy released from the reaction. The RGibbs block has been used successfully in previous studies made at the department of Energy and Environment at Chalmers to simulate combustion and gasification reactions.

The TLE was modeled using as simple heat exchanger block with the temperature of the inputs and outputs specified. The splitting columns were modeled using the separators block where the fraction of each component in the outlet stream is specified.

5.2 FBHE design

The design of the FBHE involved three steps: Geometry and dimensioning of the furnace and cracking coils, selection of bed material and related parameters, heat transfer conditions, and calculation of the required temperature level in the bed. These steps are presented in detail in the respective sections below.

5.2.1 FBHE geometry and dimensioning

The reactor coil configuration used in the base case is shown in Figure 9. Four coils are used that are placed next to each other in a single row. Combining this configuration with the dimensions of the coils given in Table 2, the length of the tube bend is approximated as the total length of the furnace minus 0.5 m from each side for tolerance and divided by the total number of bends which is 4x4=16 (tolerance reflects the physical clearance required so the tubes do not actually touch the furnace walls). Next the size of each bend is multiplied by the total number of bends (7) and subtracted from the reactor length of 100 m and divided by 8 to obtain the length of each pass in the reactor. Results are shown in Table 6.
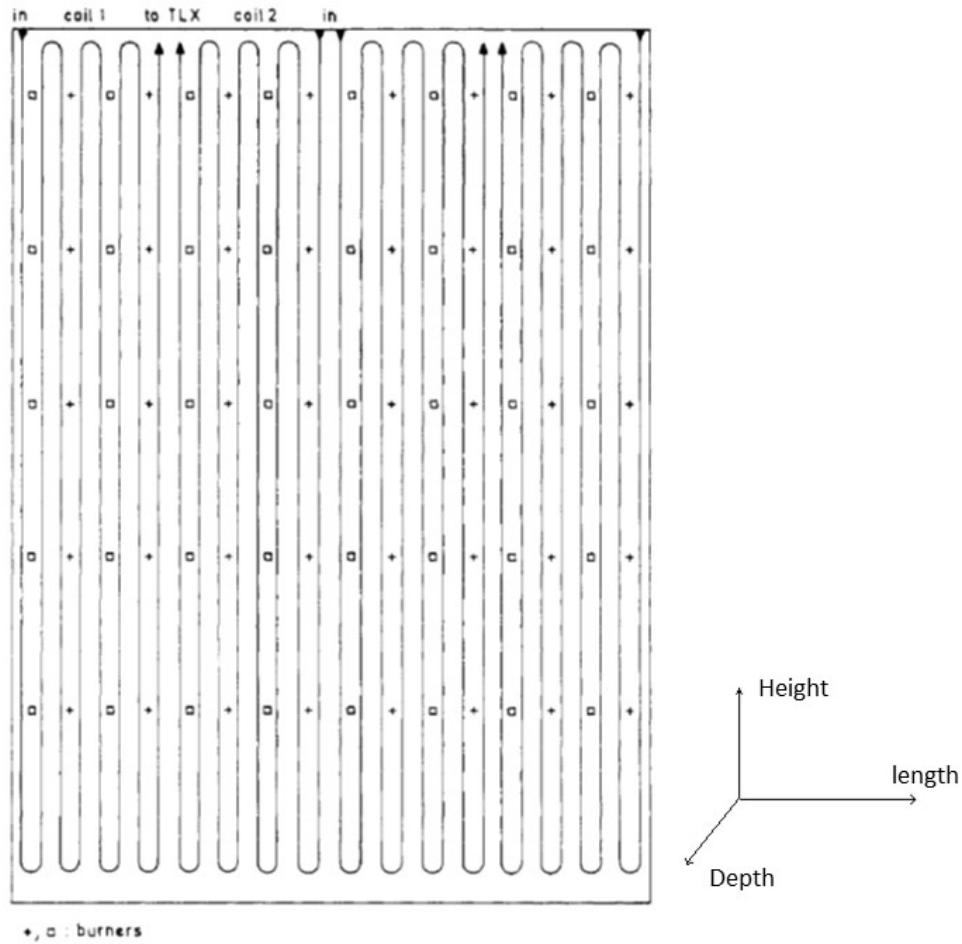
Figure 9. Reactor coil configuration in base case

Table 6.Pass and bend length

Bend length	$\dfrac{9.6 - 1}{16} = 0.534\ m$
Pass length	$\dfrac{100 - (7 * 0.534)}{8} = 12.03\ m$

In comparison with other literature studies containing plant data, the size of the reactor coil in the base case is more on the large side. As such, maintaining the same coil configuration in the FBHE where the coils should be immersed in the bed is difficult mainly due to the height of bed material that would be required and the ability to fluidize the bed. A 12 m high bed would be needed to immerse the tubes and that is not practical. Instead, the design is altered based on the fact that temperature distribution in an FBHE with OCAC is quite uniform [21] [22] and accordingly the heat transfer coefficient from the bed to the reactor tube surface is almost the same as well (one fixed value for the heat transfer coefficient). This means that the temperature profiles that exist along the

height of flame burner furnaces and the presence of secondary burners are no longer a factor for the shape and dimensions of the bed of the FBHE. Based on the above, the first modification was to stack the coils in four rows on top of each other, with each row one external diameter (15 cm) apart from the next. This means that the bed height required to immerse the tubes is 8*0.15+0.1=**1.3 m**. The bed height is an important factor for the performance of the FBHE and it directly affects bubble formation and pressure drop inside the bed. With higher bed heights the size of gas bubbles formed becomes larger which significantly decreases particle contact with the immersed tubes and hence the heat transfer. Typically bubbling fluidized beds have a height of 0.5 m. However, it is expected that the tube bundles will act as a physical barrier to bubble formation and help break the bubbles before they get too large. With respect to pressure drop, higher beds require significantly larger gas pressures to fluidize. This also means a bigger fan or compressor is needed to fluidize the bed, which means more electric power consumption.

Then the coils were shifted to a horizontal position along the length of the furnace instead of the height. In this position, the length of the FBHE required will be greater than 4*0.534= 2.1 m which is relatively small. Accordingly, to reduce the depth of the FBHE from 12 m, the number of bends and passes for each coil was increased to obtain a more square geometry. If the number of passes is increased to 14, then the tube bend number becomes 13 with a total length of 13*0.534=6.94 m and the length of the pass (depth of the FBHE) becomes **6.647 m**. The length of the FBHE is then 13*0.534=**6.94 m**. Finally, the height of the FBHE for a bubbling bed is almost the same as the height of the bed, so it was set as **1.5 m**. The new configuration in the FBHE is illustrated in Figure 10.
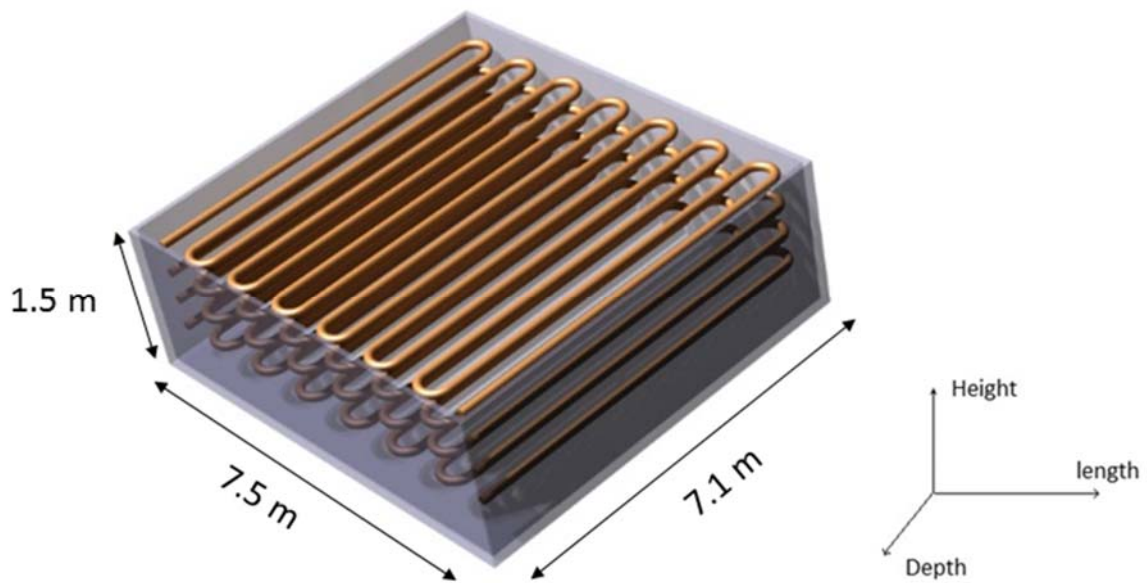

Figure 10. FBHE configuration and dimensions

Due to the high complexity of heat transfer and gas-particle flows in a FBHE, some key assumptions for the above dimensioning were considered. The effect of having coils stacked on top of each other on the heat transfer and particle contact with the tubes was assumed to be small such that the those

properties are almost the same as they would be if only one coil was immersed in the bed. This assumption stems from the study by Q.F. Hou et. al. [23] where a detailed and rigorous assessment of the effect of different tube arrangements (in-line, and staggered) on bubbling behavior and heat transfer was conducted, and no significant effect was observed. It should be noted that the study did find differences in the microscopic level but there was no specific trend for variation in heat transfer and gas-particle flows and the conclusion was that the process was too complicated and needs further research. Another assumption was that the amount of fuel that could be combusted in the FBHE and consequently the amount of energy that could be supplied was assumed to be independent of the size of the FBHE, only on the fuel and air flow rates. Finally, up to the author's knowledge there is no actual bubbling fluidized bed of the size proposed above actually in operation today. As such, the feasibility and performance of the bed was assumed to be the same as in the smaller beds on which a lot of research is available. In theory, the limiting parameter is the bed height and it has the most effect on the fluidization rather than the cross section.

5.2.2 Selection of bed material

In this study, active bed material is used in the FBHE to achieve better combustion inside the bed, more uniform temperature distribution, reduce emissions (in particular CO), and reduce power demand of auxiliary equipment due to low excess air ratios. Active bed material can be mixed with inert sand material that is typically used in fluidized beds or used as the sole bed material. Active bed material consists of metals called oxygen carriers that can chemically bond with oxygen (oxidize) and then release this oxygen (reduce) where oxygen concentrations are low. Hence the name oxygen carrier aided combustion (OCAC). With regards to performance, OCAC holds several advantages over inert bed material. Since good mixing is achieved in a fluidized bed, oxygen carriers are well distributed all over the bed. In turn, this results in more uniform oxygen availability and much better fuel and oxygen mixing which ensures complete combustion. Typically in a bubbling fluidized bed, gaseous fuels such as methane are converted to a large extent above the bed (in the freeboard), which makes it very difficult for the dense bed to reach the desired temperature and temperature distribution. The key advantage with OCAC is that oxygen carriers facilitate the conversion of fuel **inside** the dense bed. Relatively stable fuel components such as methane are combusted by direct solid-gas reactions inside the bed, where ignition may otherwise be hampered by thermal inertia [21]. Another issue is that without active bed material, higher ratios of excess air need to be used to ensure complete combustion and reduce unwanted emissions. The downside is that excess air increases the heat losses in the bed and the power consumption of support equipment such as fans. The advantage with oxygen carriers is that the ratio of excess air needed becomes much less while maintaining low CO emissions.

Several metals can serve as oxygen carriers, and the metal oxides that have been tested and found feasible are NiO/Ni, Mn_3O_4/MnO, Fe_2O_3/Fe_3O_4, Cu_2O/Cu, CoO/Co [24]. The criteria used to evaluate the oxygen carriers are listed below [24]:

- High reactivity with fuel and oxygen, and ability to convert the fuel fully to CO_2 and H_2O
- Low fragmentation and attrition, as well as low tendency for agglomeration
- Low production cost and preferably being environmentally sound

After reviewing the studies by A. Lyngfelt [24], and Ryden et. al. [21] and Kallen et. al. [25] it was found that manganese ore (Mn_3O_4) meets the above criteria quite well and experimental data on its performance is available. As such, manganese ore is adopted in this study. Since methane is used as fuel in this study, the reaction for combustion of methane is illustrated below:

$$CH_{4(g)} + 4Mn_3O_{4(s)} \rightarrow 12MnO_{(s)} + CO_{2(g)} + 2H_2O_{(g)}$$
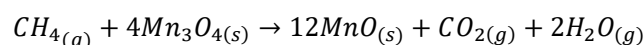
Then manganese is oxidized backed to the initial state according to the reaction below:

$$2O_{2(g)} + 12MnO_{(s)} \rightarrow 4Mn_3O_{4(s)}$$
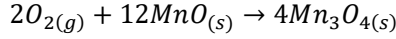
It should be noted that manganese ore batches are not solely composed of manganese, but rather a mixture of components of which manganese (Mn) holds the largest percentage (greater than 45%) [21].

Next, three more parameters were required with regards to the bed material: air-to-fuel ratio (excess air), extent of mixing of bed material, and mean particle diameter. To determine the air-to-fuel ratio and bed composition, the study by Kallen et. al. [25] was used where performance of manganese ore in a fluidized bed with methane as fuel was experimentally measured. The study showed that using a bed material with 50% manganese ore and 50% silica sand allowed the fluidized bed to be operated at an air-to-fuel ratio as low as 1.01, with CO concentrations in the flue gas about 5 times lower compared to a 100% sand bed. As such, the same bed composition was used in this paper and the excess air ratio was set to 1.03 (for practical reasons it would be difficult to operate at lower ratios). Finally, an assumption of mean particle diameter in the bed material was required for this paper as it has a significant impact on the heat transfer conditions in the FBHE as detailed in the section below. Using both Kallen et. al. [25] and Ryden et al [21], the mean diameter for a bed material consisting of sand and manganese ore was between $150 - 200 \; \mu m$. The diameter adopted in this report was $200 \; \mu m$ since it falls within the small diameter range that achieves higher heat transfer [26] [27].

5.2.3 Heat transfer conditions

The main function of the furnace in an ethylene plant is to provide heat for the endothermic reactions in the reactor tube. The FBHE serves the same function through different heat transfer mechanisms that are detailed in this section. First, the general case for heat transfer is presented. Heat transfer that occurs from the surroundings to the tube is denoted as outside/external heat transfer. Inside or internal heat transfer occurs between the tube wall and feed gases through the coke layer. Outside heat transfer occurs through convection, conduction, and radiation and the coefficients are temperature dependent. Inside heat transfer occurs mainly through conduction and is also temperature dependent. Heat transfer is represented mathematically by heat transfer coefficients which can be visualized as a resistance to the heat flow. Figure 11 illustrates the resistance concept with the different heat transfer coefficients. An overall heat transfer coefficient (h_{eq}) or equivalent coefficient can be defined to take into account all resistances. The general function for h_{eq} is shown in equation 2:

$$\frac{1}{h_{eq}} = \frac{1}{h_{out}} + \frac{d_t \ln\left(\frac{d_t}{d_i}\right)}{2k_{wall}} + \frac{d_t}{d_i} * \frac{1}{k_{coke}} + \frac{d_t}{d_i} * \frac{1}{h_i} \quad where \tag{2}$$

- $h_{out} = h_{conv} + h_{rad} + h_{cond}$
- h_{conv} : convection coefficient
- h_{rad} : radiation coefficient
- h_{cond} : conduction coefficient
- k_{wall}: tube wall conductivity
- k_{coke}: conductivity of coke layer
- h_i: coefficient for pyrolysis gas

Based on above equations, the heat transfer from the furnace to the tube will be

$$Q = h_{eq}A\left(T_f - T_g\right) \qquad (3)$$

- Q: energy consumed by the reactions for given temperature profile.
- A: surface area of reactor tube, based on outside diameter of reactor tube (d_t)
- T_f: temperature in the furnace/fluidized bed
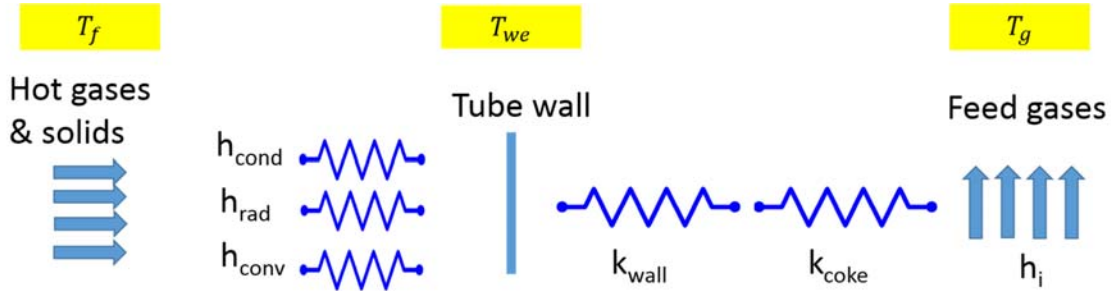- T_g: pyrolysis gas temperature inside reactor tube

Figure 11. Heat transfer coefficients analogy to electric resistance

In the FBHE surroundings include combustion gases, furnace walls, and bed material. For this study, the tubes were immersed in the bed material and accordingly were assumed not to "see" the furnace walls so no radiation from the furnace walls was considered. In addition, since the same tube and the same temperature profile for the gases was used in the FBHE, the internal heat transfer will be the same as compared to the base case. As such the outside heat transfer was the main factor and it represents the main change that occurs when using the FBHE in the process. Taking into account the outside heat transfer only, equation 3 now becomes

$$Q = h_{out}A\left(T_f - T_{we}\right) \qquad (3)$$

Equation 3 has two unknowns: h_{out} and T_f. The external tube wall temperature profile is given in Figure 8. The heat flux per unit area given in Figure 7, and integrating gives the area under the curve or the total amount of heat Q that needs to be supplied to the tube. As mentioned above, the outside heat transfer coefficients are temperature dependent, so an iterative procedure that solves for both T_f and h_{out} at the same time is required. However, the trick is finding an expression for h_{out}. The heat transfer mechanisms are very complex in a fluidized bed and are affected by many different factors that interact with each other. As such, the formulas found in literature are complicated, require detailed knowledge, and a lot of calculations to be solved without necessarily providing accurate answers. In addition, it is difficult to find a general expression for the heat transfer from a FBHE to an immersed tube that applies across all situations. To address this issue, the key factors that affect the heat transfer were identified and based on the chosen values of these factors in this paper an overall outside heat transfer coefficient value was assumed. However, a general expression for bubbling beds from Basu [28] was found to be relevant to this study and it was evaluated using common and assumed values for the different terms present. This way a calculated number for h$_{out}$ was available and can be compared to the adopted value of h$_{out}$. The expression is shown in equation 4.

$$h_0 = 900(1-\varepsilon)\frac{K_g}{d_t}\left[\frac{Ud_t\rho_p}{\mu}\frac{\mu^2}{d_p^3\rho_p^2 g}\right]^{0.326}Pr^{0.3} + \frac{\sigma(T_b^4 - T_w^4)}{\left[\frac{1}{e_b}+\frac{1}{e_w}-1\right](T_b - T_w)} \qquad (4)$$

The most important factors according to different literature reviews were the **size of the particles in the bed material (d_p), the fluidizing gas velocity or superficial gas velocity (U), and the temperature of the bed**. With smaller size particles, heat transfer to the tube is improved since the particle does not absorb a lot of heat and does not have a temperature gradient across its diameter. The diameter range for "small" particles is between 150-350 µm [27]. The fluidizing gas velocity affects the gas bubble formation and the contact time of the particles with the tube surface. Larger bubbles create a space without many particles and thus decreases heat transfer by conduction, and short contact times means the particles have limited time to transfer heat by conduction. Finally, higher temperatures in the bed create a stronger driving force for heat transfer to occur and increases the radiation contribution significantly.

To find more details and suitable values for the above factors, four papers on the topic were reviewed and compared to reach reasonable assumptions that could be applied to the case in this paper. The four papers are from Kim at al. [26], Khan et. al. [29], H-S Li et. al [30], and N. Masoumifard et. al. [31]. H-S Li et al. [30] showed that increasing temperatures in the bed result in higher heat transfer coefficients. The radiation part of the heat transfer is expected to increase quickly with higher temperatures and the radiation contribution becomes quite significant at high temperatures. The temperature required in the FBHE for steam cracking will be higher than 1000⁰C since the COT for ethane and naphtha is close to 900⁰C. Across the four papers, it was shown that heat transfer coefficients increase with smaller diameter of the sand particles. In N. Masoumifard et. al. [27] and Kim et. al. [26], it is shown that heat transfer has a maximum value at a certain U. However, a general ratio for U/U_{mf} is not defined and could be in the range of 2-4. In this paper it is assumed that the bed is fluidized at the optimum U to give the maximum heat transfer rate. In the reviewed papers, the immersed tubes had different diameters. Although the effect of this diameter is not evaluated, the values of the heat transfer coefficients obtained do not show that the diameter of the immersed tube has a direct or significant impact on the heat transfer performance of the bed. Of course using tube bundles in different configurations will affect the heat transfer properties, but for the level of detail and purpose of this paper it is assumed that this factor can be neglected. Finally, the value of the heat transfer rates measured in the four papers was compared and found to be in the range of 350-600 W/m².K. Based on the above, the operating conditions for the FBHE in this paper is compared and evaluated against the results of the literature review. Accordingly, for the given temperature and particle diameter given above the outside heat transfer rate from the FBHE to the immersed tubes (h_{out}) was assumed to be **600 W/m².K**. To further assess this assumed value, equation 4 above was used to calculate h_{out} and the value was found to be **922 W/m².K**. Based on bubbling beds in operation today, the calculated value is on the high side but it shows that the assumed value is reasonable and falls within the range between theoretical and experimental values.

To put things into perspective, the value assumed for h_{out} in the FBHE is compared with the value for flame burner furnaces found in both the base case and literature. For the base case, Figure 7 & Figure 8 were used in combination with equation 3 to find the maximum heat transfer coefficient from the furnace to the tube.

$$h_{out} = \frac{Q}{A} * \frac{1}{(T_f - T_{we})}$$

As mentioned in section 4.1 above, the difference between furnace and tube wall temperature is at maximum heat flux is around 300^0C. The maximum outside heat transfer coefficient was found to be **300 $W/m^2.K$**.

5.2.4 Temperature calculation (T_f)

The temperature level required in the FBHE is a main indicator for assessing the effect of increased heat transfer in the FBHE as compared to a typical cracking furnace. As discussed above, the temperature in the FBHE is expected to be quite uniform and constant at $T=T_f$. Furthermore, since the heat transfer coefficient from the bed to the reactor tube is also assumed constant, the external heat flux will not have the spikes and dips seen in the base case (Figure 7). Accordingly, the temperature in the FBHE was calculated using the average heat flux and the average external tube wall temperature values. Alternatively, the net heat demand can be used in conjunction with the average external tube wall temperature. Next equation 3 was used with the values of h_{out}, Q, and T_{we} to find T_f. Afterwards, h_{out} was varied over the range 300-900 $W/m^2.K$ to assess the effect on T_f and to try to further validate the chosen value of h_{out}.

6. Results and discussion

In this section the results of the calculations and sensitivity analysis are presented and discussed. A comparison is made between the furnace in the base case and the suggested FBHE.

First, a summary of the design and selected parameters for the FBHE is presented in Table 7 for easy reference.

Table 7. Summary of FBHE design and parameters

FBHE	
Length	7.34 m
Depth	7.05 m
Height	1.5 m
Bed height	1.3 m
Bed material	50% manganese ore, 50% silica sand (wt%)
Mean particle diameter (d_p)	200 μm
Excess air ratio	1.03 (kg air/kg fuel)
Outside heat transfer coefficient	600 $W/m^2.K$
Fuel	100% methane (CH_4)
Gas velocity (U)	At optimal

Next the calculation of the temperature and fuel flow rate were performed for two cases: without coke (0h) and with coke (1370h). Using the heat flux curve from Figure 8, the total heat consumed by the reactor tube was determined as the area under the curve and the units are kW/m^2. The area was based on the external tube surface, so the heat flux value obtained was multiplied by the area of the tube (based on outside diameter) and the length of the tube to get the total energy demand in MW. Since the tube has two different diameters along its length, the tube length was split into two sections accordingly. The calculation was done in MATLAB via a simple code presented in Appendix A. The formula used is shown below:

$$Q = trapz(x, y)$$

$$Q_{tot} = (Q1 * \pi * D1 + Q2 * \pi * D2)/1000$$

- trapz: MATLAB function for calculating the area under the curve
- Qtot: total energy consumed by a single reactor tube (MW)
- Q1: total heat flux for section 1 (kW/m)
- Q2: total heat flux for section 2 (kW/m)
- D1: outside diameter of section 1 = 14 cm
- D2: outside diameter of section 2 = 15.2 cm

Then the average temperature of the external tube surface was calculated for 0h (no coke) and 1370h (with coke layer). For 0h the value was 900^0C and for 1370h it was 958.4^0C. An average for the heat flux on the tube was also calculated and found to be 63.63 $W/m^2.K$. Using this average temperature and heat flux, the temperature in the FBHE can be calculated, with the assumed value of h_{out} = 600 $W/m^2.K$, as follows

$$T_{fb} = \frac{Q\_avg}{h_{out}} + Twe_{avg}$$

The results are shown in Table 8 below.

Table 8. Calculated values for T_{fb} based on different cases

T_{fb} based on average T_{we} for 0h	1006 ^0C
T_{fb} based on average T_{we} for 1370h	1064 ^0C

It can be seen that the temperature in the fluidized bed needs to be approximately 106^0C higher than the external tube wall temperature to provide the necessary heat demand. Figure 12 a) illustrates the heat flux profile and average heat flux while b) shows Twe_{avg}, T_{we} profile, and T_{fb} for the 1370h scenario.
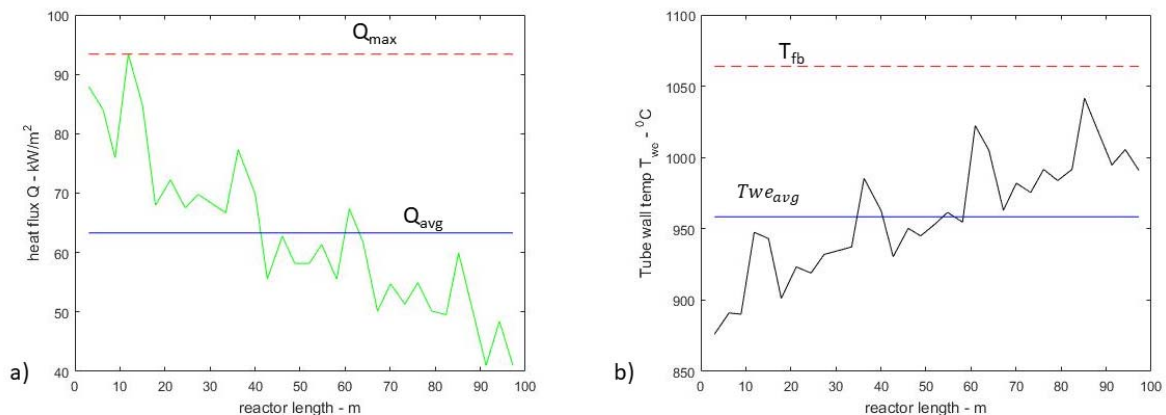

Figure 12. a) heat flux and average heat flux for 1370h, b) external tube wall temperature profile T_{we}, T_{we} average, and fluidized bed temperature for 1370h

As for the total heat required by the reactor tube, the heat consumed in one reactor tube for 0h was **2.58 MW** and **2.6 MW** for 1370h. Since four reactor tubes are present, the total heat demand from the furnace and FBHE becomes 4*2.6=**10.4 MW**. The two values are almost the same as expected since the temperature profile inside the reactor tube was kept almost the same as shown in Figure 6. The slightly higher value at 1370 h was used for the fuel consumption calculations.

To find the mass flow rate of fuel needed, the combustion reaction for CH_4 was considered at the temperature of the furnace or FBHE coupled with the excess air ratio used in each case. The energy released by the combustion reaction per kg of burnt fuel was calculated as the enthalpy difference between the products and reactions. Then the mass flow rate is the energy consumed in the reactor tube divided by the energy released per kg of burnt fuel.

Using the fuel flow rate, excess air ratio, and temperature in the furnace and FBHE the CO emissions were determined using the RGibbs block in Aspen Plus. The data obtained for the furnace are summarized in Table 9 and for the FBHE in Table 10.

Table 9. Summary of obtained parameters for the furnace of the base case

At 0 h (no coke)	
$\dot{m}_{fuel}$	0.5503 kg/s
Excess air ratio	1.2
Total Q consumed by reactor tubes	10.4 MW
T_f	1183 ^{0}C
CO concentration in flue gas (mol basis)	1.32 ppm
At 1370 h (with coke deposit)	
$\dot{m}_{fuel}$	0.6226 kg/s
Excess air ratio	1.2
Total Q consumed by reactor tubes	10.4 MW
T_f	1258 ^{0}C
CO concentration in flue gas (mol basis)	4.16 ppm

Table 10. Summary of obtained parameters for FBHE

At 0 h (no coke)	
$\dot{m}_{fuel}$	0.3073 kg/s
Excess air ratio	1.03
Total Q consumed by reactor tubes	10.4 MW
T_{fb}	1006 ^{0}C
CO concentration in flue gas (mol basis)	1.17 ppm
At 1370 h (with coke deposit)	
$\dot{m}_{fuel}$	0.3206 kg/s
Excess air ratio	1.03
Total Q consumed by reactor tubes	10.4 MW
T_{fb}	1064 ^{0}C
CO concentration in flue gas (mol basis)	4.19 ppm

From the above tables, the effect of improved heat transfer conditions in the FBHE can be evaluated. It can be seen that the temperature required in the FBHE is **177^{0}C** lower than the furnace at 0h and **194^{0}C** lower at 1370h. This temperature difference, in addition to lower excess air, results in about **44.1%** lower fuel consumption in the FBHE at 0h and about **48.5%** lower at 1370h. The values presented above also reflect the effect of coke deposition on the operation of the FBHE. The temperature difference between no coke and with coke is **58^{0}C** in the FBHE which in turn results in **4.33%** more fuel consumption.

The ethylene yield in all cases for both the furnace and the FBHE was the same since the same temperature and pressure profiles were applied to the reactor tube. The ethylene yield, ethane conversion, and CH_4 yield were obtained from the Aspen Plus model. Yield was defined as the weight of the product divided by the weight of the ethane feed. A comparison between the obtained values and the values in the base case was also performed. The results are summarized in Table 11 below.

Table 11. Ethane conversion and ethylene and CH_4 yields

	Base Case	Simplified kinetic model	Percentage difference
Pressure in	292 kPa		
Pressure out	195 kPa		
COT	850 ^{0}C		
Ethane conversion	63.4 %	72%	8.6 %
Ethylene yield	48 wt%	53.3 wt%	5.3 %
CH_4 yield	4.3 wt %	5.93 Wt %	1.63 %

6.1 Sensitivity Analysis

In this section the effect of different "variables" on the "results" is evaluated. The findings are illustrated in graphs and then discussed to shed more light on both the operating conditions in the FBHE and the ethane steam cracking process.

6.1.1 Outside heat transfer coefficient in FBHE (hout)

The heat transfer coefficient in the FBHE was varied between 300 and 900 W/m^2.K to determine the effect on temperature in the FBHE and fuel consumption. The results are shown in Figure 13 and Figure 14 below.
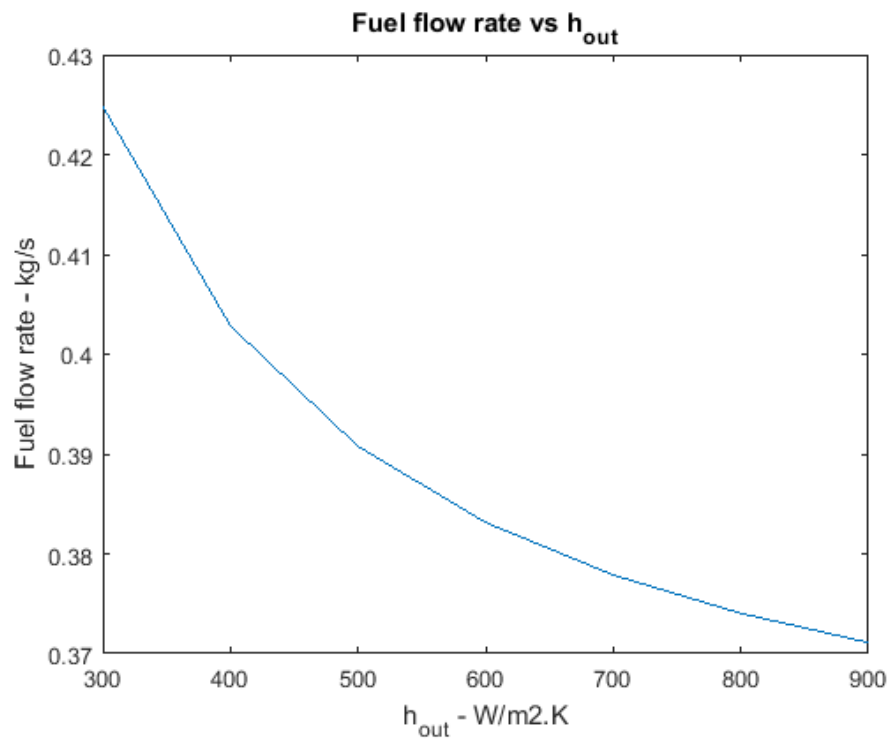

Figure 13. Effect of external heat transfer coefficient on fuel consumption in the FBHE

From the respective figures, if h_{out} is increased from the adopted 600 to 900 W/m^2.K, fuel consumption can be decreased by around **3.7%** while the temperature required in the FBHE will decrease by around **35^{0}C**. It can also be noted that the slope of the lines decreases with increasing heat transfer coefficient, meaning that the savings in fuel consumption and decrease in temperature is much higher when going from 300 to 600 than it is from 600 to 900.
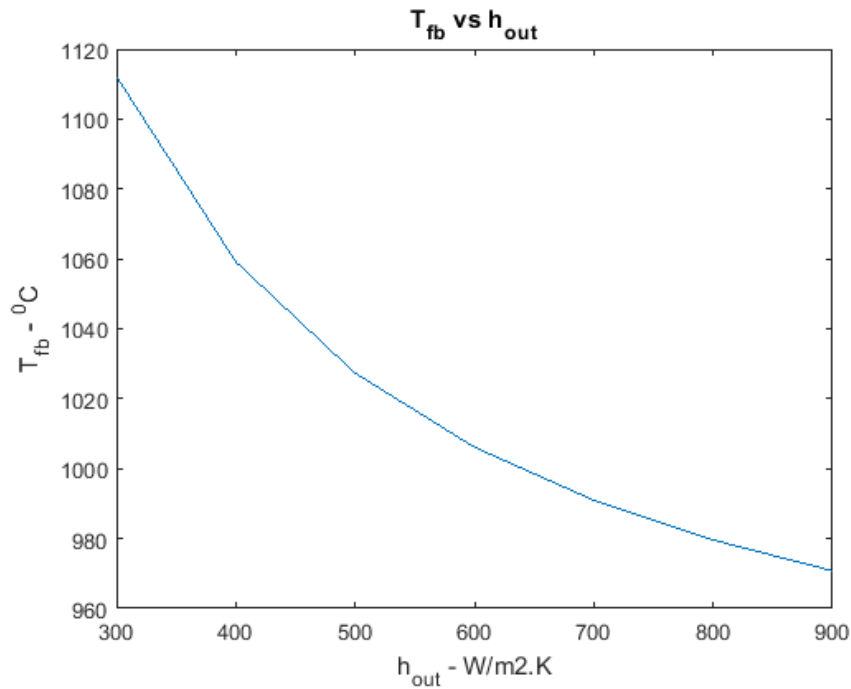
Figure 14. Effect of external heat transfer coefficient on temperature in the FBHE

6.1.2 Steam to hydrocarbon ratio

The steam to hydrocarbon ratio (S/HC) is varied from 0.2-0.8 kg steam/kg ethane. The variation is done in Aspen Plus on the reactor tube block. The main effect of this variation was found to be on the ethylene yield. Figure 15 shows the effect of the steam to hydrocarbon ratio on ethylene yield.
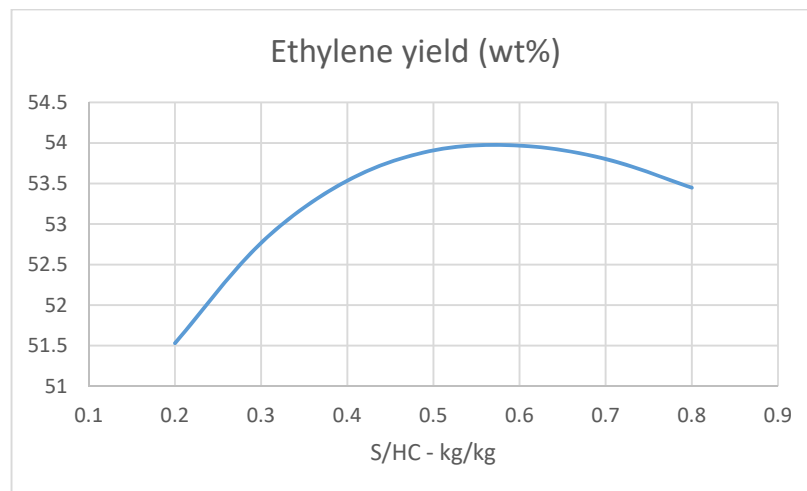

Figure 15. Ethylene yield vs S/HC

It can be seen from Figure 15 that the yield improves with higher steam to hydrocarbon ratios up to a certain maximum, after which the yield actually starts to decrease. As such, there is an optimum range for the S/HC ratio between 0.5 and 0.6 kg/kg. The S/HC ratio used in the base case paper was

0.365 kg/kg. Another benefit of increased steam dilution is a reduction in the coke layer formed inside the reactor tube. However, it should also be mentioned that more steam comes at an increased energy cost.

6.1.3 Coil outlet temperature (COT)

The coil outlet temperature is typically used as an indicator to the temperature levels in the reactor tube since it is relatively easier to measure that temperature. In this study, each point on the temperature profile of the reactor tube was adjusted by the same amount as the change in COT. The main effect of COT were observed in the ethylene yield and energy consumption in the reactor tube. The results are shown in Figure 16 and 17.
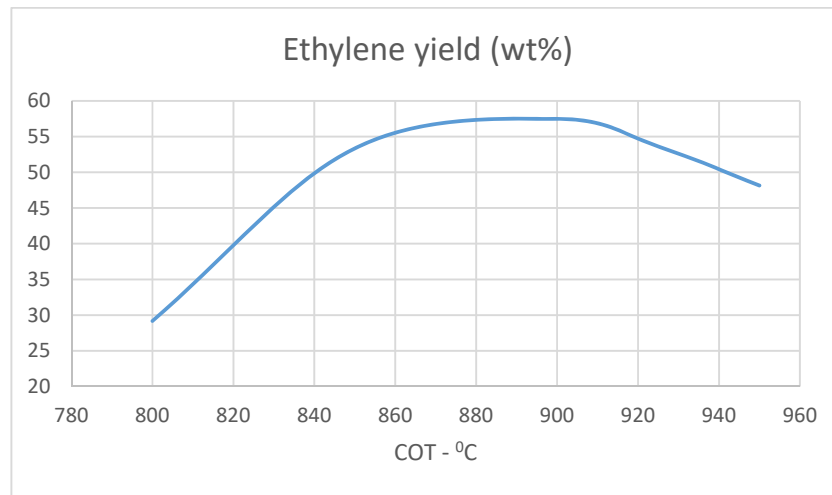

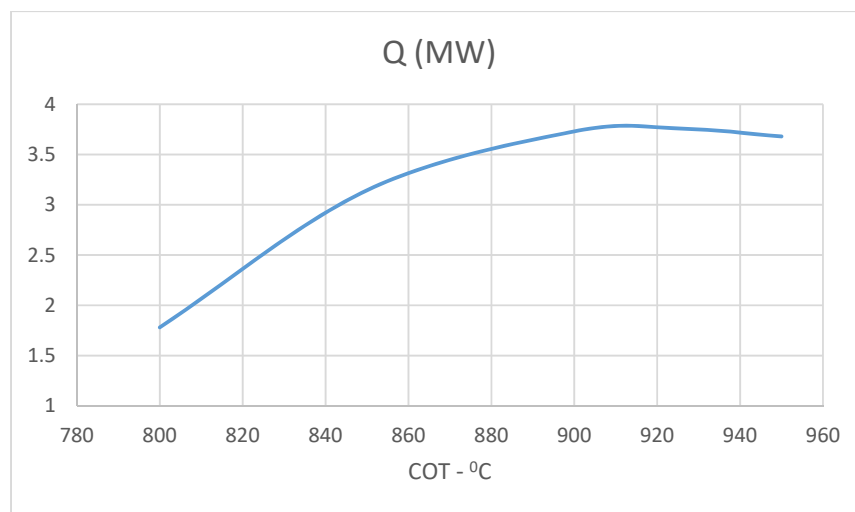
Figure 16. Ethylene yield vs COT

Figure 17. Energy consumption in reactor tube vs COT

37

From the above figures, it can be seen that there is an optimum range of COT at which ethylene yield is maximized. The optimum range is between 860 and 910^{0}C. At temperatures higher than the optimum range, the ethylene yield decreases rapidly. A possible explanation for the decrease in yield could be that ethylene conversion reactions into other products becomes faster at these high temperatures. Looking at the energy consumption, the trend is an increase in energy demand with increasing temperatures, again up to a point where the energy consumption stagnates and begins to decrease slightly. Since this coincides with the ethylene yield trend, this signifies that ethane conversion into ethylene is possibly the most energy intensive reaction in the cracking process. On another note, increase in COT will also lead to more coke deposits which shortens the run length of the furnace or FBHE.

6.1.4 Pressure of the feed

The pressure of the feedstock is known to have an effect on the yields, and as such was varied from 220-320 kPa. The results are shown in Figure 18 below.
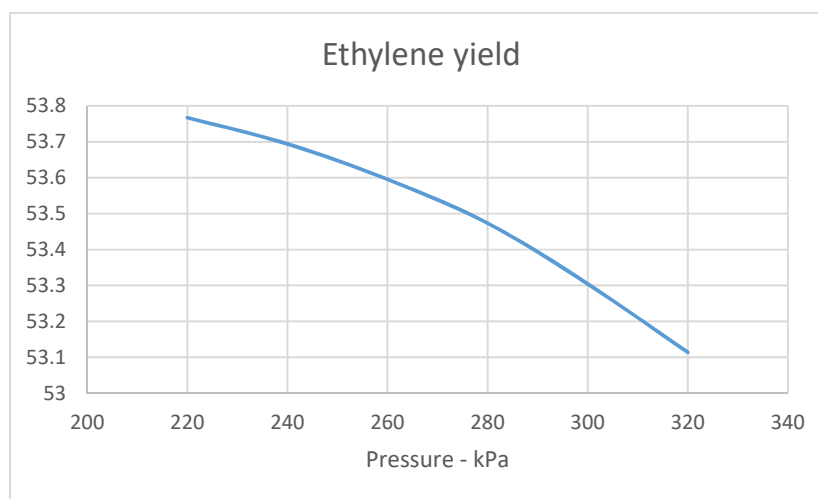

Figure 18. Ethylene yield vs feedstock pressure

It can be seen that lower pressures increase the ethylene yield, so conversion reactions to ethylene are favored at lower pressures.

7. Conclusions

This study has shown that a fluidized bed heat exchanger with oxygen carrier aided combustion has superior heat transfer potential compared to the typical flame burner furnace used in steam cracking processes. The improved heat transfer in the FBHE-OCAC can save a significant amount of fuel, and with it the energy demand. In addition, temperatures required are much lower in the FBHE compared to the flame burner furnace. Lower temperature mean lower heat losses from the furnace or FBHE and less heat stress on the material present. Furthermore, lower excess air ratios due to the oxygen carrier bed material saves energy requirements for auxiliary equipment which further enhances the total efficiency of the process. Based on the results, there is room for more energy savings if the design of the FBHE is optimized with respect to the key parameters affecting the heat transfer. However, the sensitivity analysis showed that higher values of h_{out} have a decreasing impact on the temperature and fuel consumption. One possible explanation is that the outside heat transfer starts approaching the internal heat transfer rate, making the internal rate the limiting factor.

For the Aspen plus model, the results show that the model is suitable for predicting yields and assessing the effect of operating conditions on the product output. The model also reflects an overview of an ethane steam cracking plant, showing the different stages present in the steam cracking process. As such, the model allows for further more detailed development of both the reaction kinetics and downstream processes where a complete energy assessment of the plant can be performed. The sensitivity analysis on the reactor tube showed that the coil outlet temperature (COT) has the biggest effect on ethylene yield, reflecting the highly endothermic nature of the cracking reactions. The pressure of the feed had the lowest impact on ethylene yields. In addition, there is an optimum range of operation for the steam to hydrocarbon ratio and COT at which the ethylene yield is maximized.

Recommended future research is to create an experimental setup or pilot plant to test the FBHE-OCAC and take measurements that can be used to further validate and improve the accuracy of the results of this study. It is suggested to involve industry in future research in order to optimize the steam cracking process using the FBHE and develop new methods or tools to take advantage of the benefits brought by the FBHE. Another important work would be an economic evaluation of an FBHE-OCAC compared to the typical flame burner furnace where costs and profits can be compared.

References

[1]   I. E. A. (IEA), "Tracking Industrial Energy Efficiency and CO2 emissions," 2007.

[2]   S. Sadrameli, "Thermal/catalytic cracking of liquid hydrocarbons for the production of olefins: A state-of-the-art review II: Catalytic cracking review," *Elsevier,* 2016.

[3]   S. AG, "Process Analytics in Ethylene Production Plants," 2007.

[4]   M. Eramo, "Global Ethylene Market Outlook: Low Cost Feedstocks Fuel The Next Wave Of Investments In North America and China," IHS Chemical - Technip, 2013.

[5]   S. Sadrameli, "Thermal/catalytic cracking of hydrocarbons for the production of olefins: A state-of-the-art review I: Thermal cracking review," *Elsevier,* 2014.

[6]   M. Bender, "An Overview of Industrial Processes for the Production of Olefins - C4 Hydrocarbons," *ChemBioEng Reviews,* 2014.

[7]   H. ZIMMERMANN and R. WALZL, Ethylene, Wiley-VCH Verlag GmbH & Co, 2009.

[8]   M. Magyarorszag, 2005. [Online]. Available: https://mol.hu/images/pdf/A_MOL_rol/tvk-rol/tarsasagunkr%C3%B3l_roviden/egyetemi_kapcsolatok/debreceni_egyetem/oktatasi_anya gok/bemutatok/OLEFINS%20PRODUCTION.pdf.

[9]   A. N. et. al, "The combined simulation of heat transfer and pyrolysis reactions in industrial cracking furnaces," *Applied Thermal engineering,* 2004.

[10]   S. et. al., "Simulation and optimization of a Naphtha thermal cracking pilot plant," *Iran journal of Chemistry and chemical engineering,* 2003.

[11]   T. D. c. company, 2017. [Online]. Available: http://www.dow.com/hydrocarbons/c4/prod/cc4.htm.

[12]   M. Shokrollahi Yancheshmeh, S. Seifzadeh Haghighi, M. Gholipour, O. Dehghani, M. Rahimpour and S. Raeissi, "Modeling of ethane pyrolysis process: a study on effects of steam and carbon dioxide on ethylene and hydrogen productions," *Chemical Engineering Journal,* 2012.

[13]   P. M. Plehiers, G. C. Reyniers and G. F. Froment, "Simulation of the run length of an ethane cracking furnace," *Industrial & engineering chemistry research,* 1990.

[14]   M. Ramana Rao, P. M. Plehiers and G. F. Froment, "The coupled simluation of heat transfer and reaction in a pyrolysis furnace," *Chemical engineering science,* 1988.

[15]   R. P. et. al, "Modeling of ethane thermal cracking kinetics in a pyrocracker," *Chemical Engineering Technology,* vol. 35, 2012.

[16]   G. Hu, H. Wang, F. Qian, K. M. Van Geem, C. M. Schietekat and G. B. Marin, "Coupled simulation of an industrial naphtha cracking furnace equipped with long-flame and radiation burners," *Computers and Chemical Engineering, 38,* 2012.

[17] H. Guihua, W. H. gang and F. Qian, "Numerical simulation on flow, combustion and heat transfer of ethylene cracking furnaces," *Chemical Engineering Science, 66,* 2011.

[18] K. Sundaram and G. F. Froment, "Modeling of thermal cracking kinetics-I: thermal cracking of ethane, propane, and their mixtures," *Chemical Engineering Science,* 1976.

[19] M. Rosli and N. Aziz, "Simulation of ethane steam cracking with severity evaluation," *IOP conference series: Material Science and Engineering 162,* 2017.

[20] J. Towfighi, J. Modarres, M. Omidkhah and A. Niaei, "ESTIMATION OF KINETIC PARAMETERS OF COKING REACTION RATE IN PYROLYSIS OF NAPHTHA," *IJE transactions B,* 2004.

[21] M. Rydén, F. Lind, M. Hanning and A. Corcoran, "Oxygen Carrier Aided Combustion (OCAC) of Wood Chips in a Semi-Commercial Circulating Fluidized Bed Boiler Using Manganese Ore as Bed Material," *Applied Sciences 6, 347,* 2016.

[22] M. RYDÉN, M. HANNING and F. LIND, "Improved combustion in fluidized bed with manganese ore as bed material," *ENERGIFORSK,* 2016.

[23] Q. Hou, Z. Zhou and A. Yu, "Gas–solid flow and heat transfer in fluidized beds with tubes: Effects of material properties and tube array settings," *Powder Technology 296,* 2016.

[24] A. Lyngfelt, "Oxygen Carriers for Chemical Looping Combustion - 4 000 h of Operational Experience," *Oil & Gas Science and Technology – Rev. IFP Energies nouvelles, Vol. 66,* 2011.

[25] M. Källén, M. Rydén and F. Lind, "Improved Performance in Fluidised Bed Combustion by the Use of Manganese Ore as Active Bed Material," *22nd International conference on fluidized bed conversion (FBC),* 2015.

[26] S. W. Kim, J. Y. Ahn, S. D. Kim and D. H. Lee, "Heat transfer and bubble characteristics in a fluidized bed with immersed horizontal tube bundle," *International Jounral of Heat and Mass Transfer 46,* 2003.

[27] N. Masoumifard, N. Mostoufi, A.-A. Hamidi and R. Sotudeh-Gharebagh, "Investigation of heat transfer between a horizontal tube and gas–solid fluidized bed," *International Journal of Heat and Fluid Flow, 29,* 2008.

[28] P. Basu, Combustion and gasification in fluidized beds, Taylor & Francis, 2006.

[29] R. TURTON and T. KHAN, "The measurement of instantaneous heat transfer coefficients around the circumference of a tube immersed in a high temperature fluidized bed," *International journal of heat and mass transfer, vol 35,* 1992.

[30] L. HONG-SHUN, Q. REN-ZHANG, H. WEN-DI and B. KAI-JUN, "An investigation on instantaneous local heat transfer coefficients in high-temperature fluidized beds-l. Experimental results," *International journal of mass and heat transfer, vol 36,* 1993.

[31] S. A. Deshmukh, S. Volkers, M. van Sint Annaland and H. Kuipers, "Heat Transfer in a Membrane Assisted Bubbling Fluidized Bed with Immersed Horizontal Tubes," *INTERNATIONAL JOURNAL OF CHEMICAL REACTOR ENGINEERING, Vol 3,* 2005.

[32] G. L. A.Chauvel, Petrochemical processes: Synthesis-Gas derivatives and major hydrocarbons, Institut Francais du petrole publications, 1989.

[33] S. Gundur, "RATE-BASED MODELING OF STEAM ETHANE CRACKER," Middle East Technical University, 2015.

[34] M. K. Sabbe, K. M. Van Geem, M.-F. Reyniers and G. B. Martin, "First principle-based simulation of ethane steam cracking," *American Institue of Chemical Engineers,* 2011.

Appendix A – MATLAB code for temperature calculation and sensitivity in FBHE

```
clear all
close all
% Q curve for 1370 h
Q_coke=[87.95 84.04 75.96 93.39 84.77 67.95 72.23 67.52 69.79 66.67 77.31
69.79 55.54 62.75 58.17 58.17 61.35 55.54 67.40 61.71 50.15 54.74 51.31
54.92 50.15 49.54 59.94 40.98 48.44 40.98];
x=[3.05 6.26 8.94 11.86 15.03 17.87 21.21 24.47 27.39 33.49 36.24 40.04
42.71 46.05 48.81 52.03 54.78 58.12 60.92 63.97 67.18 70.06 73.24 76.12
79.21 82.42 85.18 91.27 94.24 97.24];
x1=[3.05 6.26 8.94 11.86 15.03 17.87 21.21 24.47 27.39 33.49 36.24 40.04
42.71 46.05 48.81 52.03 54.78 58.12 60.92 63.97 67.18 70.06 73.24];
x2=[76.12 79.21 82.42 85.18 91.27 94.24 97.24];
Q_coke1=[87.95 84.04 75.96 93.39 84.77 67.95 72.23 67.52 69.79 66.67 77.31
69.79 55.54 62.75 58.17 58.17 61.35 55.54 67.40 61.71 50.15 54.74 51.31];
Q_coke2=[54.92 50.15 49.54 59.94 40.98 48.44 40.98];

%Q curve for 0 h
Q_0h=[78.72 75.96 67.40 86.30 77.55 61.83 67.58 63.79 65.44 66.79 63.12
77.31 69.79 55.54 62.75 58.17 58.17 61.35 55.54 73.52 68.62 52.84 58.17
55.11 58.72 52.97 70.21 45.69 53.33 46.85];
x_0h=[3.01 6.26 9.06 12.07 15.03 18.12 21.21 24.47 27.39 30.48 33.82 36.24
40.04 42.71 46.05 48.81 52.03 54.78 58.12 60.79 63.72 67.47 70.19 73.24
76.20 82.17 85.34 91.52 94.57 97.62];
x11=[3.01 6.26 9.06 12.07 15.03 18.12 21.21 24.47 27.39 30.48 33.82 36.24
40.04 42.71 46.05 48.81 52.03 54.78 58.12 60.79 63.72 67.47 70.19 73.24];
x22=[76.20 82.17 85.34 91.52 94.57 97.62];
Q11=[78.72 75.96 67.40 86.30 77.55 61.83 67.58 63.79 65.44 66.79 63.12
77.31 69.79 55.54 62.75 58.17 58.17 61.35 55.54 73.52 68.62 52.84 58.17
55.11];
Q22=[58.72 52.97 70.21 45.69 53.33 46.85];
figure
plot(x,Q_coke)
hold on
plot(x_0h,Q_0h)
%Area under the curve 1370h = total kW/m for each tube section
Q1=trapz(x1,Q_coke1);
Q2=trapz(x2,Q_coke2);
%tube surface area
A1=pi()*0.14;
A2=pi()*0.152;
%Total energy consumed by reactor tube for 1370h (MW)
Q_tot=((Q1*A1)+(Q2*A2))/1000;

%Area under the curve 0h = total kW/m for each tube section
Q1h=trapz(x11,Q11);
Q2h=trapz(x22,Q22);
%Total energy consumed by reactor tube for0h (MW)
Q_toth=((Q1h*A1)+(Q2h*A2))/1000;

%Twe profiles for t=0h and t=1370h
Twe_0h=[845.03 858.70 853.11 895.65 891.61 864.29 878.57 875.78 882.61
887.58 915.53 901.55 882.30 896.58 892.86 894.10 903.11 901.55 933.85
924.53 904.35 915.22 914.60 918.32 918.94 917.08 948.45 925.78 933.23
926.71];
Twe_1370h=[876.09 890.99 890.06 947.52 943.17 901.24 923.29 918.94 931.99
937.27 985.40 962.73 930.43 950.31 945.03 953.42 961.49 954.66 1022.36
```

```matlab
1004.97 963.04 981.99 975.47 991.61 983.85 991.61 1041.61 994.72 1005.59
990.99];
%Temperature profile inside reactor tube
x_value=[0 4.9 9.8 14.7 19.6 24.5 29.4 34.3 39.2 44.1 49 53.9 58.8 63.7
68.6 73.5 78.4 83.3 88.2 93.1 98];
y_value=[656 693.17 718.55 736.12 743.71 752.82 760.63 767.35 776.68 780.15
786.66 791.87 798.37 807.70 810.74 816.38 822.89 828.31 840.02 843.49 850];
figure
plot(x_value,y_value,'g',x,Twe_0h,'r',x,Twe_1370h,'b')
%find average Twe for each time period
Twe_avg=mean(Twe_0h);
Twe_avg2=mean(Twe_1370h);
%find Tfb (fluidized bed temp)
Qavg=mean(Q_0h);
Qavg2=mean(Q_coke);
Tfb=(Qavg*1000)/600 + Twe_avg;
Tfb2=(Qavg2*1000)/600 + Twe_avg2;
%find point wise Tf and Tfb for 0h
Tf=(Q_0h./300)*1000 + Twe_0h;
Tfb_0h=(Q_0h./600)*1000 + Twe_0h;
figure
plot(x,Tf);
hold on
plot(x,Tfb_0h);
plot(x,Twe_0h);
furnace_temp=max(Tf)+273;
fb_temp=max(Tfb_0h)+273;
Tfb_avg=mean(Tfb_0h);
%find point wise Tf and Tfb for 1370h
Tf2=(Q_coke./300)*1000 + Twe_1370h;
Tfb_coke=(Q_coke./600)*1000 + Twe_1370h;
figure
plot(x,Tf2);
hold on
plot(x,Tfb_coke);
plot(x,Twe_1370h);
furnace_temp2=max(Tf2)+273;
fb_temp2=max(Tfb_coke)+273;
Tfb_avg2=mean(Tfb_coke);
%data for CH4 combustion
h_ch4=-74980;
H_CO2 = -394088;
H_H2O = -242174;
T_in=298;
l=[1.2 1.03 1.2 1.03];
T=[furnace_temp Tfb furnace_temp2 Tfb2];
Q_total=Q_toth*4;
%calculate m.dot for Tf and Tfb at corresponding lambdas
for i=1:4

lambda=l(i);
n_N2_p  = 2*lambda*3.76;
n_O2_p  = 2*(lambda-1);



T_out=T(i);
H_r=1*h_ch4;
H_p = H_CO2 + 2*H_H2O + (T_out-T_in) * (1*44.3191 + 2*32.4766 +
n_N2_p*29.2313 + n_O2_p*30.5041) + ((T_out)^2-(T_in)^2)/2 * (1*0.00730 +
2*0.00862 + n_N2_p*0.00307 + n_O2_p*0.00349);
Q_2(i)=H_r-H_p; %J/mol
```

```matlab
Q_extract(i)=Q_2(i)*62.5; %J/kg fuel
m_fuel(i)=(Q_total*1e6)/Q_extract(i); %kg/s
i=i+1;
end

%sensitivity for h_out
H_out=[300 400 500 600 700 800 900];
n_N2_p  = 2*1.03*3.76;
n_O2_p  = 2*(1.03-1);
for j=1:7
    h_out=H_out(j);
    temp(j)=(Qavg/h_out)*1000 + Twe_avg;

    %temp(j)=(Q_coke./h_out)*1000 + Twe_1370h;
    T_out2=temp(j)+273;
    H_r=1*h_ch4;
    H_p = H_CO2 + 2*H_H2O + (T_out2-T_in) * (1*44.3191 + 2*32.4766 +
n_N2_p*29.2313 + n_O2_p*30.5041) + ((T_out2)^2-(T_in)^2)/2 * (1*0.00730 +
2*0.00862 + n_N2_p*0.00307 + n_O2_p*0.00349);
    Q_3(j)=H_r-H_p; %J/mol
    Q_extract2(j)=Q_3(j)*62.5; %J/kg fuel
    m_dot(j)=(Q_total*1e6)/Q_extract2(j);
end

figure
plot(H_out,temp)
title('T_f_b vs h_o_u_t')
xlabel('h_o_u_t - W/m2.K')
ylabel('T_f_b - ^0C')
figure
plot(H_out,m_dot)
title('Fuel flow rate vs h_o_u_t')
xlabel('h_o_u_t - W/m2.K')
ylabel('Fuel flow rate - kg/s')
```

Appendix B – Aspen Plus model flowsheet screenshot